Bulletin of the New Zealand Society for Earthquake Engineering, Vol. 58, No. 4, December 2025

SEISMIC FRAGILITY OF MASONRY INFILLED REINFORCED CONCRETE FRAMES UNDER IN-PLANE LOADING: A HYBRID EXPERIMENTAL AND NUMERICAL APPROACH

Siyavur Raheem[1], Julian Thamboo[2], Chinthaka Mallikarachi[3], Kushan Wijesundara[4] and Priyan Dias[5]

(Submitted *October 2024*; Reviewed *January 2025*; Accepted *February 2025*)

ABSTRACT

Many experimental studies have been conducted to understand the in-plane behaviour of reinforced concrete frames infilled with masonry walls (IM-RC). However, detailed analyses of those experimental studies have revealed that the in-plane behaviour of certain IM-RC frame configurations (e.g. different masonry strengths, wall aspect geometries, high strength masonry infills with ductile frames) are not well explored. Therefore, an attempt has been made to extend the understanding of the in-plane behaviour of IM-RC frames by analysing different IM-RC frame configurations using experimental and numerical data. Focus was given in this study to analyse the in-plane behaviour of single storey-single bay IM-RC frames. The numerical analyses were conducted on specific IM-RC frame cases, where experimental results are not available. For that purpose, a numerical modelling method employing fibre-element based RC frames with multi-diagonal struts for IM walls was used. The established numerical modelling method of IM-RC frames has been validated with different experimental datasets, thus proving its ability to accurately predict the in-plane behaviour of different IM-RC frames. Using the experimental and numerical datasets created, a set of seismic fragility functions have been developed. Four damage states incorporating evolution from IM to RC failures have been defined. The fragility functions are given in terms of compressive strengths of IMs (≤ 5MPa, > 5 & ≤15 MPa, and >15 MPa), and type of RC frame used (non-ductile and ductile). The derived fragility functions clearly show the importance of designing ductile frames for IM-RC building types; and the combinations of high strength IM walls with non-ductile RC frame configurations are shown to be more vulnerable than the other IM-RC frame configurations analysed.

https://doi.org/10.5459/bnzsee.1718

INTRODUCTION

The reinforced concrete (RC) frame infilled with masonry walls is a very popular typology used to design low to medium rise buildings around the world. Masonry walls are generally used to provide internal partitions and external facades in RC framed buildings, as they offer good sound and thermal insulation, and provide aesthetic appeal. In moment resisting frames designed for only gravity load combinations (e.g. buildings in low and moderate seismic regions, or pre-code buildings in high seismic regions), the infill masonry (IM) walls are considered as non-structural elements, and their masses are only accounted in the design as permanent actions. It is well understood now that the IM wall can interact with the surrounding frame, when the frame is subjected to lateral action [1-2]. The IM walls create additional thrust forces to the surrounding frame under lateral actions, and those thrust forces acting close to the beam-column joint region (in fully infilled frames) and directly on columns if the frame is partially infilled [3-4]. If the surrounding frame is not designed for those additional thrust forces, shear failure of columns or failure at beam-to-column joints can occur, and this can lead to partial/complete brittle failure (i.e. short column effect) [5-6]. Vertical and horizontal irregularities (mass and stiffness) created by irregular arrangement of IMs would induce torsional force and soft-storey problems in IM-RC buildings [7-9]. The deficiencies in seismic detailing in RC elements (including beam-to-joints and columns), combined with thrust forces induced by IMs, would make the masonry infilled reinforced concrete (IM-RC) frames prone to earthquakes [10-11].

Substantial experimental, analytical and numerical studies have been conducted to comprehend the performance of IM-RC frames under seismic loading over the past five to six decades [12-13], where special attention was given to understand the in-plane performance of IM-RC frames. The out-of-plane failure of IM walls is a localised phenomenon, as the failure is limited to IM walls, rather than the frame [14-15]. The in-plane behaviour of IM-RC is not only related to IM walls, but also associated with the in-plane behaviour of surrounding frame systems. Hence the load resisting mechanism under in-plane action is more complex than out-of-plane behaviour of IM walls. In order to better understand the interaction between IM and surrounding RC frames under seismic loading, many experimental studies have been conducted by testing single storey-single bay RC frames under low fatigue cyclic in-plane loading [16-18]. Also, a few more studies have been carried out on multi-storey IM-RC frames under in-plane cyclic, pseudo-dynamic and shake-table loading conditions [19-22]. The key factors that influence the in-plane behaviour of IM-RC frames such as type of masonry, configurations of masonry (fully filled or partially filled with opening) and type of frame (non-ductile and ductile frames) were investigated in those experimental programs [23-24], which have generated a wealth of experimental data on the in-plane behaviour of IM-RC combinations.

Several researchers have developed experimental databases of IM-RC frames tested under in-plane loading conditions and analysed them to better understand the behaviour of IM-RC frames. Sassun et al., [25] characterised the in-plane seismic

[1] *Graduate Student, Department of Civil Engineering, University of Moratuwa*
[2] *Corresponding Author, Senior Lecturer, Department of Civil Engineering, South Eastern University of Sri Lanka, jathamboo@seu.ac.lk*
[3] *Professor, Department of Civil Engineering, University of Moratuwa*
[4] *Professor, Department of Civil Engineering, University of Peradeniya*
[5] *Emeritus Professor, Department of Civil Engineering, Sri Lankan Institute of Information Technology*

performance of single storey-single bay IM-RC/steel frames using 182 experimental datasets. A set of analytical functions to model an equivalent single strut of IM for the macro modelling method was developed based on this database. Liberatore et al., [26] used 162 experimental datasets of single storey-single bay IM-RC/steel frames to calibrate and propose a new set of equivalent single strut analytical functions to represent IM walls for macro level analyses of IM-RC buildings. Noh et al., [27] verified three different hysteretic models against the experimental datasets of single storey-single bay IM-RC frames to propose the most suitable hysteretic model for macro analyses of IM-RC buildings. Romano et al., [28] investigated the uncertainties in using different IM strut models to determine the seismic performances of IM-RC buildings. De Risi et al., [29] have used quite a similar approach to calibrate equivalent single strut analytical functions, but focusing only on IM-RC frame datasets made of hollow clay masonry units. Also, Huang et al., [30] used 264 datasets including IM frames made of RC and steel to develop empirical functions to define back-bone curves for IM using multivariate regression. Similar approaches have been used by some other researchers to establish better empirical and analytical functions to represent the IM wall as (an) equivalent strut/s in RC frames, and can be referred in Haindl et al., [31], Srechai et al., [32], Sirotti et al., [33], and Mucedero et al., [34].

In addition, some researchers used a similar set of databases to develop empirical fragility functions for IM-RC frames under in-plane loading conditions. Cardone and Perrone [35] used 55 experimental datasets of IM-RC frames to develop fragility and loss functions only for IM components. Del Gaudio et al., [36] followed a similar approach to develop fragility functions, but using 136 datasets of IM-RC frames made of clay brick and concrete block masonry. Chiozzi and Miranda [37] incorporated 152 datasets comprised of frames made of RC and steel to derive empirical fragility and loss functions. Recently, Xie et al., [38] tested nine IM-RC frames made of concrete block masonry, and derived empirical fragility functions using the experimental results. However, the damage states defined to derive the fragility functions and associated loss functions differ in these studies. Their appropriateness in defining the in-plane damage sequences of IM-RC frames under in-plane loading is discussed in Section 2. Although extensive experimental datasets of IM-RC frames are available, a closer examination of those datasets reveals that there are gaps in knowledge in terms of the IM-RC configurations examined under in-plane seismic actions - more details on these aspects are outlined in Section 3. In particular, not all types of masonry used as infills are experimentally investigated. In addition, differences in RC frame types in terms of having ductile or non-ductile detailing, along with other mechanical parameters of IMs and geometries, are not explicitly examined. Hence, there is a need to improve the dataset of IM-RC frames, from which more appropriate fragility functions under in-plane seismic actions can be developed.

This study was aimed to extend the understanding of in-plane behaviour of against the experimental datasets of single storey-single bay IM-RC frames with different combinations of IM-RC frame configurations using experimental databases and numerical analyses; thus a data generating hybrid approach was followed. For this purpose, an extensive experimental database of single storey-single bay IM-RC frames was initially established, with 157 sets of experimental results gathered. The database was analysed to comprehend the in-plane behaviour of IM-RC frames with varying parameters, such as masonry properties, geometries and RC configurations. It was found that certain IM-RC frame configurations have not been tested through experimental studies. Therefore numerical analyses of IM-RC frames were specifically carried out for those unexplored IM-RC frames configurations. The numerical analysis procedure developed to analyse IM-RC frames using OpenSees (OS) [39] that incorporates multi-struts to represent the IM, and fibre elements to characterize the RC elements through axial-flexural-shear interaction mechanisms. Subsequently, using the experimental and numerically generated data, seismic fragility functions have been established. It can be said that this study has extended the knowledge on the in-plane characteristics of IM-RC frames with different IM and RC configurations, as well as enhanced the seismic fragility functions through a more comprehensive data generated via experimental and numerical methods.

DEFINITIONS OF DAMAGE STATES

Seismic fragility functions define the probability of a structural system exceeding predefined damage limit states during envisaged seismic actions. Therefore, the damage limit states for a structural system need to be defined properly, in order to have fragility functions that are related to such specific damage. This will enable the better assessment of vulnerability and determination of seismic losses. Defining damage states for IM-RC frames is quite challenging due to the involvement of different structural elements (i.e. IM and RC frame) and their interactions. The performance of IM-RC frames tend to vary with the relative strength/displacement characteristics of IM walls and RC elements. Some efforts have been made to develop specific damage limit states for IM-RC frames under in-plane loading and are outlined in Table 1. Also, some standards such as ASCE 41 [40] and EN 1998-1-1 [41] provide rational damage limit states that include IM-RC moment resisting frames. All these definitions of damage limit states correspond to immediate occupancy (negligible damage, sometimes referred to as operational), damage limitation (minor damage), life safety (significant damage) and near collapse (collapse prevention) of structures in the aftermath of a seismic event. However, the approaches to define these performance levels against damage states differ among the studies considered.

Cardone and Perrone [35] defined four damage limit states as given in Table 1, considering only the damages of IMs (in-plane and out-of-plane failures), using an experimental database of single storey-single bay IM-RC frames. Chiozzi and Miranda [37] also proposed three damage limits for IM-RC frames using an experimental database, also linked only to the damage to IMs, as these studies were focused on assessing the non-structural losses in IM-RC frames. Del Gaudio et al., [36] also used the same damage limit states proposed by Cardone and Perrone [35] using an extended experimental database of IM-RC frames. Sassun et al., [25] also utilised four damage limit states, again involving only IMs, to develop fragility curves from an experimental database of IM-RC frames. Jeon et al., [42] developed a set of fragility functions specifically for lightly reinforced IM-RC frames as outlined in Table 1 using numerical analyses.

Rossetto and Elnashai [43] have incorporated the failure sequence of the frame along with the IMs to define the damage states at global scale. Since the failure is dependent on the mechanical and geometrical properties of IM as well as the surrounding frame, the authors are of the opinion that the damage states to define the IM-RC frames under in-plane loading should incorporate the failure sequence of both elements (IM and RC frame). The 157 datasets of IM-RC single storey-single bay frames analysed (explained in Section 3) also reflect that the failure sequence of IM-RC frames starts from damage initiation in IM, followed by RC elements, ending up with shear or flexural failure in RC frames.

Table 1: Damage states defined in previous studies.

References	Damage States			
Sassun et al., [25]	**DS1:** Detachment of IM from the frame and minor cracking on IM	**DS2:** Damage to the IM, through the formation of bi-diagonal cracking, Very limited crushing and spalling of few units	**DS3:** Cracks and sliding of joints and cracks in the masonry units. The IM is not repairable at reasonable costs	**DS4:** The IM is close to collapse
Cardone and Perrone [35] & Del Gaudio et al., [36]	**DS1:** Separation of IM from the frame, and their crack width is less than 1 mm	**DS2:** Extensive diagonal cracking about 2 mm on IM and possible failure of masonry units at 10% of IM area	**DS3:** Spalling of masonry units (nearly 30%), corner crushing, spalling of plaster, sliding of mortar joints. Repair of IM is not feasible	**DS4:** In-plane or out-of-plane collapse of IM
Chiozzi and Miranda [37]	**DS1:** Cracking of plasters and hairline cracks in IM, up to 2 mm near the columns and/or near the top beam	**DS2:** More than 2 mm wide cracks in IM. Common repair actions required are the removal of cracked IM and replacement of IM	**DS3:** Wider diagonal cracks on IM more than 4 mm width, significant sliding of joints and widespread damages to masonry units. Repairing the IM is not economically feasible	
Jeon et al., [42]	**DS1:** Cracking of IM and limited crushing of masonry units. No noticeable damage to the surrounding frame	**DS2:** Wider cracks on the IM and initiation of yielding of flexural reinforcement in the frame	**DS3:** Collapse of IM and flexural failure of frame	
Rossetto & Elnashai [43]	**DS1:** Minor separation of IM from the frame. Diagonal cracking of IM. Limited crushing of masonry units at upper corners	**DS2:** Increased crushing of masonry units at upper corners. Start of structural damage. Diagonal shear cracking of RC members at exterior frames	**DS3:** Extensive IM cracking, falling masonry bricks, OOP bulging, partial IM failure, heavier damage in frame members	**DS4:** Near total IM failure. RC member failure in shear

Hence, the damage states provided by Rossetto and Elnashai [43] are considered to be more appropriate for IM-RC frames, if the vulnerability and losses (from both structural-RC frame and non-structural-IMs) of the entire buildings are to be analysed [44-45]. Other studies have only focused on loss assessment via non-structural damages (i.e. damages to IMs), and have overlooked the damages to the RC frame in developing fragility functions. Though the damage states defined in Rossetto and Elnashai [43] are for global scale, they are still applicable at single storey-single bay IM-RC frames (at local level), as they incorporate the damage sequence of IMs and RC frame. The proposed damage states could be used in numerical analyses of IM-RC frame to develop fragility functions, and also as an empirical tool. Hence, those damage states (reflecting damage in both IMs and RC frames) have been used to develop fragility functions from the IM-RC database created in this study. More details on retrieving the data from the experimental studies to establish fragility functions according to the damage states are given in Section 3.

IM-RC FRAME DATABASE

The experimental datasets created of IM-RC frames tested under in-plane loading conditions is explained in this section. The single storey-single bay IM-RC frame testing results in the literature under monotonic and cyclic in-plane loading have been collected, as those results provide unambiguous insight on the interaction between IM and RC under in-plane loading and their failure sequences, as opposed to the multi-storey IM-RC frames tested. Although the multi-storey IM-RC frames/prototype buildings tested under in-plane cyclic, pseudo-dynamic and shake-table loading conditions enable better understanding of the global behaviour of these building typologies, the IM-RC frame configurations tested in those conditions are unique in their own configurations [38-39]; hence such data are not appropriate for focusing on the influence of IM and RC configurations under in-plane cyclic loading, which is the objective of this study. In total, 157 datasets of fully filled IM-RC frames tested under in-plane loading were gathered from 50 studies and summarised in Table 2. Some of the experimental data (particularly the older research data) in the literature were not included, as they do not give adequate information on the lateral load-displacement curves and associated failure sequences of the IM-RC frames sought in this study. The experimental database developed is given in ***Supplementary data A*** (see the online version).

Categorisation of the Database

The information retrieved from the selected IM-RC frames tested were: (1) type of masonry (e.g. clay brick, concrete block, and autoclaved aerated concrete (AAC) block), (2) mechanical properties of masonry (e.g. compressive strength, and shear strength), including the properties of their constitutive materials (i.e. strengths of masonry units and mortars, if provided), (3) geometries of IM-RC frames (i.e. length, height and thickness of IM walls and cross-sectional dimensions of beam and columns used), and (4) reinforcement configurations used in RC elements (longitudinal and transverse reinforcement ratios used in beams and columns). Figure 1 shows the categorisation of the database according to the parameters considered. Some of the past studies have only focused on assessing the in-plane behaviour of IM-RC frames according to masonry properties and greatly overlooked the contribution of RC frame characteristics to the in-plane resistance mechanisms of IM-RC frames. The majority of past studies have varied the RC element sizes (i.e. frame types) and corresponding detailing with IM types to examine the in-plane effects. Hence, the IM-RC frames

in the database have been categorised only in terms of type of IM, geometry of wall and reinforcement detailing used. Properties of steel bars used in the frames (157 datasets) have not significantly varied. Therefore, the RC cross-sectional details, including their reinforcement arrangements used in past studies have been incorporated for detailed analyses.

Categorisation According to Constitutive Strengths

The IM-RC frames were initially categorised into the type of IM used in terms of masonry compressive strengths (f_m). The f_m is generally determined using masonry prism testing methods, while some of the results have used masonry wallette testing methods. To generalise the f_m of masonry used, all the prism compressive strengths were converted to wallette compressive strengths as per the method outlined in Thamboo and Dhanasekar [46], since wallette masonry specimens represent more realistic strength characteristics of masonry. Subsequently, IMs in the database were classified into three ranges of f_m, namely (1) $f_m \leq$ 5MPa, (2) 5 MPa < $f_m \leq$ 15 MPa and (3) f_m > 15 MPa, with these ranges are regarded as low, medium and high strength masonry assemblies [47]. The datasets were further subdivided into strength of concrete (fc) used in the frames as (1) $f_c \leq$ 50 MPa and (2) f_c> 50 MPa, representing frames made of normal and high strength concrete as per EN 1992-1-1 [48]. The concrete strengths used in the experimental studies considered varied between 9.6 to 56 MPa. Since only ten datasets were available for f_c > 50 MPa, and it was decided to not separately analyse the in-plane behaviour of IM-RC with fc > 50 MPa. The scope of the study was limited to analysing in-plane behaviour and fragility functions specific to IM-RC frames in low-rise buildings (where normal strength concrete would be used).

Categorisation According to IM Geometry

The datasets (subdivided according to the material properties) were further categorised into the geometry of IMs used, i.e. the aspect (*h/l*) and slenderness (*h/t*) ratios. Only the IMs categorised as per *h/l* ratios are shown in Figure 1 according to *h/l*≤1 and *h/l*>1, as it is generally perceived that the masonry walls with lower aspect ratios show more shear dominant failure (diagonal cracking and sliding), with the higher aspect ratios failing by flexural dominant modes (rocking or corner crushing) [49]. As per EN 1996-1-1 [50], the maximum allowable slenderness limit of unreinforced masonry walls could be 27, and the database was classified according to this slenderness limit as well; however, all the IMs used complied with this slenderness limit. Thus, slenderness was not analysed as a separate category in this study

Categorisation According to RC Frame Types

Next, the IM-RC frames included in the database were further categorised into the type of RC frames tested, for which purpose the RC frames were divided into two types, i.e. (1) non-ductile and (2) ductile. Although the non-ductile or ductile detailing of a RC frame is dependent on the seismic demand and ductility/performance criterion assumed in the design [51-52], in this study the RC frames were categorised according to reinforcement detailing followed, based on conformity to the provisions stipulated in EN 1998-1-1 [41]. Based on the detailing provided in the IM-RC frame testing programs, the RC frames were initially classified according to longitudinal reinforcement ratio (ρ_v) provided, which has to be more than 1.0% for ductile frames; otherwise, the frames are regarded as non-ductile.

The datasets were further divided by the amount of transverse reinforcement provided in the columns of IM-RC frames tested. For columns, it is specified that the transverse reinforcement should be spaced according to Eq (1) in the critical region, and an amount of reinforcement provided as per Eq (2) to create adequate triaxial confinement to the core concrete of the columns - given in EN 1998-1-1 [41]. Relevant details were retrieved from the RC frame detailing provided and the IM-RC frames categorised accordingly. The RC frames that do not comply with either Eqs (1) and (2), or do not have ρ_v of more than 1.0%, are regarded as non-ductile frames; however where all three criteria are simultaneously compiled, such frames are considered as ductile in the database created. It has to be mentioned that the IM-RC frames were not further categorised according to the specific detailing in beams and beam-column joints, since such explicit sectional detailing is not generally provided in some studies; also, for IM-RC frames, the column detailing is presumed to be more critical in resisting the thrust forces created by IMs.

$$s = min\left\{\frac{b_0}{2}; 175\ mm; 8d_l\right\} \quad (1)$$

$$\alpha\omega_{wd} \geq 30\mu_\varphi v_d \varepsilon_{sy,d} \frac{b_c}{b_0} - 0.035 \quad (2)$$

Here, s, b_0, b_c, d_l, ω_{wd}, μ_φ, v_d, $\varepsilon_{sy,d}$, and α are spacing of stirrups, width of section, width of core concrete, minimum diameter of the longitudinal bar, mechanical volumetric ratio, curvature ductility factor, normalised axial force, design value of tension steel strain at yield, and confinement factor, respectively. Volumetric ratio, ω_{wd} is the ratio of the volume of confining hoops to that of the concrete core. Curvature ductility factor, μ_φ was assumed to be 2. The confinement effectiveness factor, α depends on spacing of confining bars and geometry of the column. It has to be mentioned that the anchorage details at beam-to-column joints, and deficient rebar splicing lengths pertaining to non-ductile or ductile categorisations were not examined in this study, as such detailing is not explicitly described in the past experimental studies reported.

Gaps in the IM-RC Database

The complete categorisation of the IM-RC testing data is shown in Figure 1, where the whole database is divided into type of IM, geometry of IM, and details of RC frame used. Nearly, 51.6% of the IM-RC frames tested were constructed with masonry strength less than 5 MPa, whereas only 21.7% of IM-RC frames consist of masonry strengths more than 15 MPa. In terms of aspect ratios of IMs, most of the IM-RC frames had aspect ratios of *h/l*<1 (79.6%), while limited studies have used IM aspect ratio more than 1.0. In addition, it can be noted that most of the RC frames tested had vertical reinforcement ratios less than 1.0%, in combination with non-ductile confinement detailing as explained in Section 3.1.3; hence those IM-RC frames are regarded as non-ductile frames. In contrast, only a few IM-RC frames tested contain vertical reinforcement more than 1.0% and ductile confinement detailing. These observations reveal that, although plenty of experimental studies are available on the in-plane behaviour of IM-RC frames, certain parameters that influence in-plane behaviour are not well explored. Therefore, it implies that further studies are needed to comprehend the entire spectrum of in-plane behaviour of IM-RC frames with different IM and RC frame characteristics.

Table 2: Summary of experimental database created.

No	References	Number of IM-RC frames tested
1	Leuchar & Scrivener [53]	1
2	Zarnic & Tomazevic [54]	2
3	Kao et al., [55]	4
4	Angel [56]	8
5	Haider [57]	8
6	Mehrabi et al., [58]	12
7	Combescure et al., [59]	2
8	Crisafulli [60]	2
9	Calvi & Bolognini [61]	9
10	Lafuente et al., [62]	10
11	Choi et al., [63]	2
12	Huang et al., [64]	2
13	Bergami [65]	3
14	Altin et al., [66]	1
15	Kakaletsis & Karayannis [67]	3
16	Xu et al., [68]	2
17	Imran & Aryanto [69]	3
18	Starvdis [70]	1
19	Tizapa [71]	3
20	Waly [72]	3
21	Baran & Sevil [73]	3
22	Yuksel & Teymur [74]	3
23	Mansouri et al., [75]	2
24	Morandi et al., [76]	4
25	Bose & Rai [77]	3
26	Sigmund & Penava [78]	2
27	Cavleri & Trapani [22]	13
28	Bergami & Nuti [79]	3
29	Schwarz et al., [80]	7
30	Misir et al., [81]	3
31	Jiang et al [82]	7
32	Dehghani et al., [83]	2
33	Gazic & Sigmund [84]	14
34	Basha & Kaushik [85]	9
35	Huang et al., [86]	5
36	Alwashali et al., [87]	3
37	Cai & Su [88]	2
38	Morandi et al., [89]	4
39	Dautaj et al., [90]	8
40	Ismail et al., [91]	2
41	Akhoundi et al., [92]	5
42	Sen et al., [93]	1
43	Binici et al., [94]	4
44	Han et al., [95]	2
45	Deng et al., [96]	2
46	Sakr et al., [97]	2
47	Lu & Zha [98]	2
48	Xie et al [99]	7
49	Aydin et al., [100]	2
50	Demiral et al., [101]	2

Retrieving In-Plane Load-Displacement Data for IM-RC Frames

The in-plane drift levels of tested IM-RC frames associated with the Rossetto and Elnashai [43]'s damage states defined in Section 2 were gathered from the experimental results reported. Some experimental studies have clearly explained the failure sequences of each MI-RC frame tested under in-plane loading; hence their corresponding drift levels were directly retrieved. However, certain studies did not explicitly explain the in-plane failure sequences of IM-RC frames tested; hence their drift levels corresponding to each damage state considered were gathered from the load-displacement curves reported. For this reason, the load-displacement curves of the experimental studies were digitalized using an open sourced image processing tool, WebPlotDigitizer [102]. Backbone curves were derived from the digitalized in-plane hysteresis curves reported in the experimental studies, and using those backbone curves the drift levels corresponding to damage states were obtained. The process of deriving the backbone curves from the experimental hysteresis curves and assigning the drift levels are illustrated in Figure 2. Then the backbone curves were idealised as tri-linear load-displacement curves as per the method outlined in previous studies [103-104], such that both (actual and idealized) curves possessed equal dissipated energy. Consequently, the yield, peak and ultimate points of the load-displacement curves were defined

Since, four damage states (DSs) were considered in study, they are correlated to the load-displacement curves of the IM-RC frame retrieved. When explicit information was not provided in the studies, DS1 is defined as the 50% of the linear elastic branch of the load-displacement curves, where minor hairline cracks in IM and slight separation of IM from the frames are generally observed. Based on the analyses of the database, at about 50% of the linear-elastic line, the IMs only show initiation of cracks that could be repaired with mortar grouting/re-plastering. Thus, 50% of the linear-elastic limit is not the complete damage of IM; it indicates the initiation of damage (cracks) in IMs that could be repaired easily. DS2 is considered at the yield point defined in the backbone curve (i.e. initiation of nonlinear behaviour), where is shown to be significantly cracked the IM and the RC frame contributes (i.e. longitudinal reinforcement in the columns) to the load resisting mechanism. At the peak point of the idealised load-displacement curves, the IM is considered to be fully cracked, and visible cracks appear in general at portions of the frame. DS4 was set to the ultimate point of the load-displacement curves as the collapse of IM portions and severe cracking of the frame (flexural/shear at columns or beams-column joints) that are generally observed in the experimental programs. These points considered in the load-displacement curves can be related to the Rossetto and Elnashai [43] damage states defined in Section 2. The drift values corresponding to these DSs were retrieved from the idealized load-displacement curves, and used to establish fragility functions.

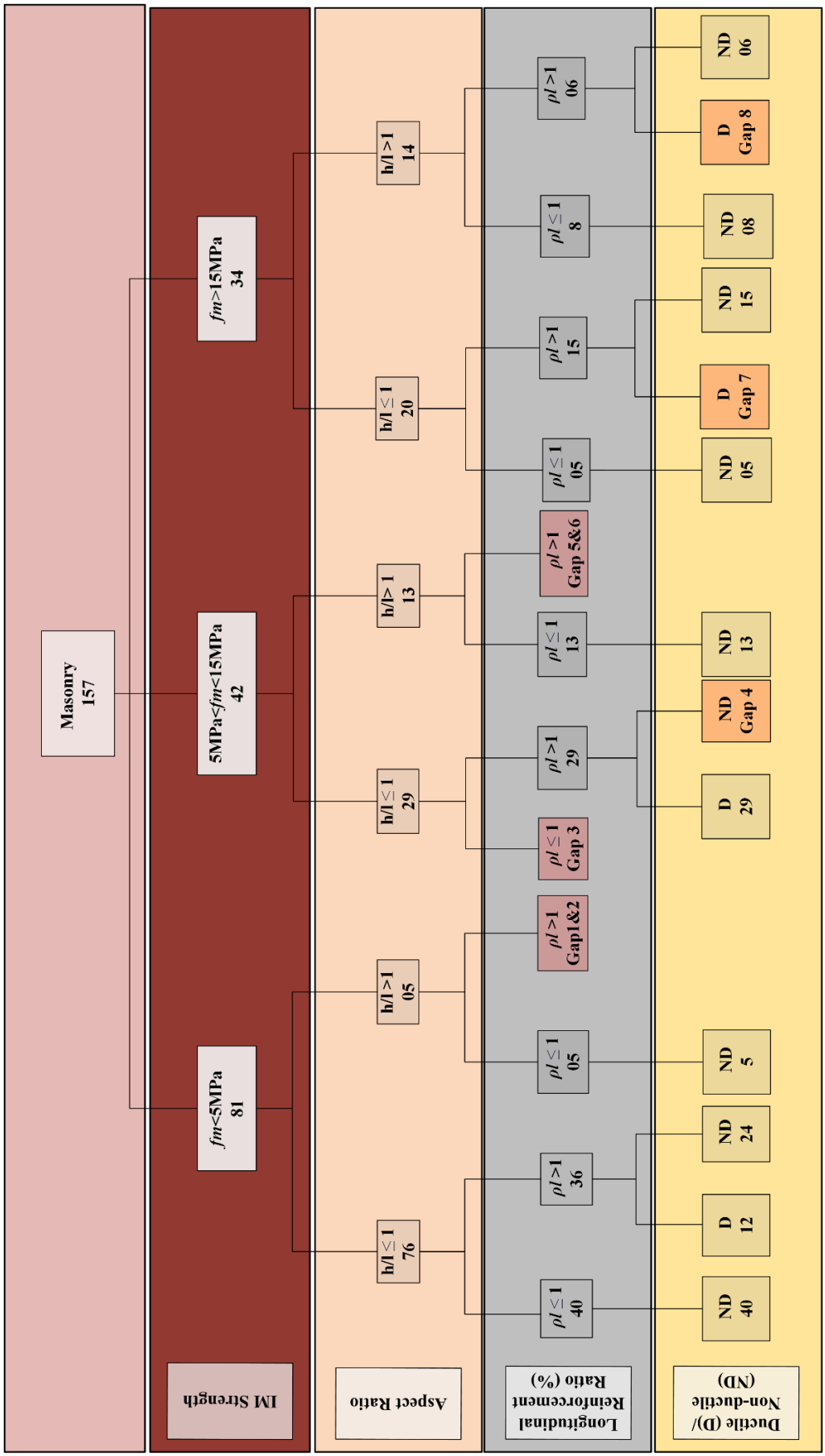

Figure 1: Categorisation of the IM-RC experimental database, showing gaps in the data.

EXTENSION OF IM-RC DATABASE

The categorisation of the experimental database revealed that although many studies have been conducted to study the in-plane behaviour of IM-RC with various IM and frame types, gaps still prevail for understanding the in-plane behaviour of certain IM-RC frame configurations. Therefore the fragility functions developed in the past studies from the existing experimental database could be covering only certain IM-RC frames. As such, the IM-RC database is extended in this study by numerically analysing the missing IM-RC frame configurations, thus filling gaps in the experimental data, in order to establish appropriate fragility functions. The details of the numerical method developed to analyse the IM-RC frames under in-plane cyclic loading and the validation of the numerical modelling method are explained in the following sub-sections.

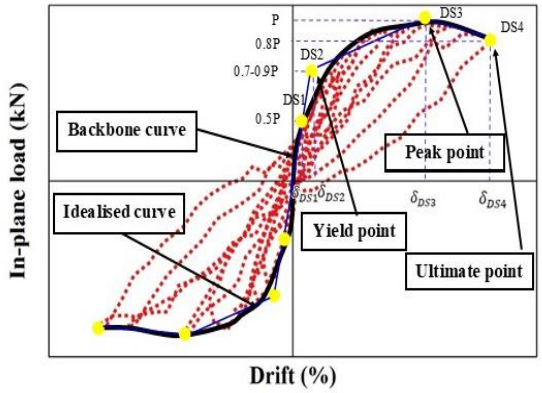

Figurer 2: Retrieving the backbone curves and assignment of drift levels corresponding to damage states.

Numerical Modelling of IM-RC Frame

To numerically model the IM-RC frame under in-plane loading conditions, the finite element based macro modelling approach was selected and simulated through OS [39]. Although the macro modelling approach is generally used to analyse the global behaviour of IM-RC frames, recent developments in using the OS [39] framework have been shown to provide adequate information on the element level load-resistance mechanisms in addition to global load-deformation responses. A typical IM-RC frame modelled through OS [39] is schematically shown in Figure 3.

A fiber based distributed plasticity approach was used, which allows inelastic behaviour by discretizing elements into fibers and along the deformable region of the member length. This modeling approach also has the benefit of capturing the axial-moment (P-M) interaction of elements. RC fiber sections were modelled using *Concrete07* and *Steel02* uniaxial material models available in the OS [39] portfolio to capture the non-linear hysteretic characteristics in the cross-sections. This Concrete 07 material model is comprised of hysteresis curves, which has the advantage of considering the confined effect on the concrete core area. To represent the steel portions, the Steel 02 material model was used, which has the benefit of considering the isotropic-strain hardening. Five integration points have been used for each fiber section with the nonlinearBeamColumn element. The bond-slip between the steel and concrete was simulated using the (Bond SP01 material) within the OS [39].

Shear failure at end of the column and beam section is considered to be the critical failure mode in the IM-RC frames. In moment resisting frames, generally shear forces are maximum near column and beam ends. Moreover, IMs also tend to create additional thrust forces to column ends (which depends on the relative stiffness between IMs and columns). Considering all these factors, the shear failure at beam and columns ends needs to be modelled. For this purpose, zeroLengthSection elements have been used at each column and beam as shown in the Figure 3. To determine shear backbone curves for the zeroLengthSection elements to capture the shear failure at columns and beams, the Response-2000 [105] sectional analysis tool was used. The shear capacities and backbone curves of the RC columns and beams were determined using Response-2000 [105], which is based on the Modified compression field theory [106], and shown to be a more appropriate way of assigning shear backbone behaviour for RC sections than the empirical based Elwood's model [107]. Hence, the shear backbone curves were derived for each frame analysed using Response-2000 [105], and assigned to zeroLengthSection elements used in them. The analysis was stopped when the shear failure in the columns were detected, and the corresponding load-displacement curves were used to determine the characteristics of the IM-RC frames. More details on determining these shear capacities of RC sections and the way it incorporates axial- flexural-shear interactions can be referred to in Rajapakse et al., [108] and Sathurshan et al., [109]. In addition, the geometrical non-linearity in the columns was considered by P-Delta transformation in the IM-RC frames modelled.

The IM in the frame is represented using a two strut approach; hence better interactions between IM and surrounding frame could be simulated. The two strut modelling approach outlined in Srechai et al., [110], which was improved from Burton and Deierlien [111] has been incorporated in modelling IMs in this study. One of the diagonal struts was connected between beam-column joints, and other was offset from the joints as shown in Figure 3. Truss elements were used to model IM. The zero tension Concrete01 material was assigned to the IM struts. This material can capture global response of IM to a reasonable accuracy with limited parameters. The way these material properties are assigned is explained in the next section. The force and stiffness distribution of the struts are adopted from Noh et al., [27]. Of the total stiffness, 75% is assigned to the diagonal strut, while the 25 % to off-diagonal strut, as specified in Srechai et al., [110].

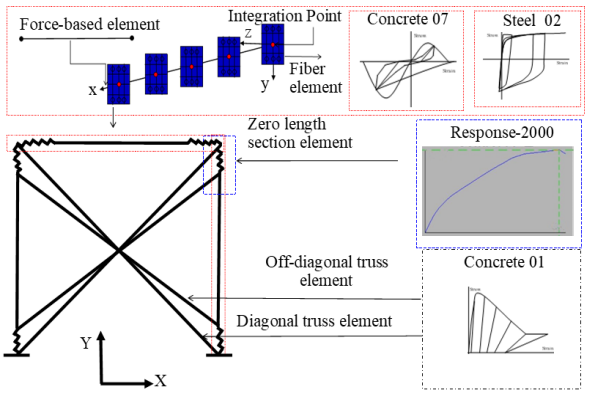

Figure 3: IM-RC frame modelling concept adopted through OS [39].

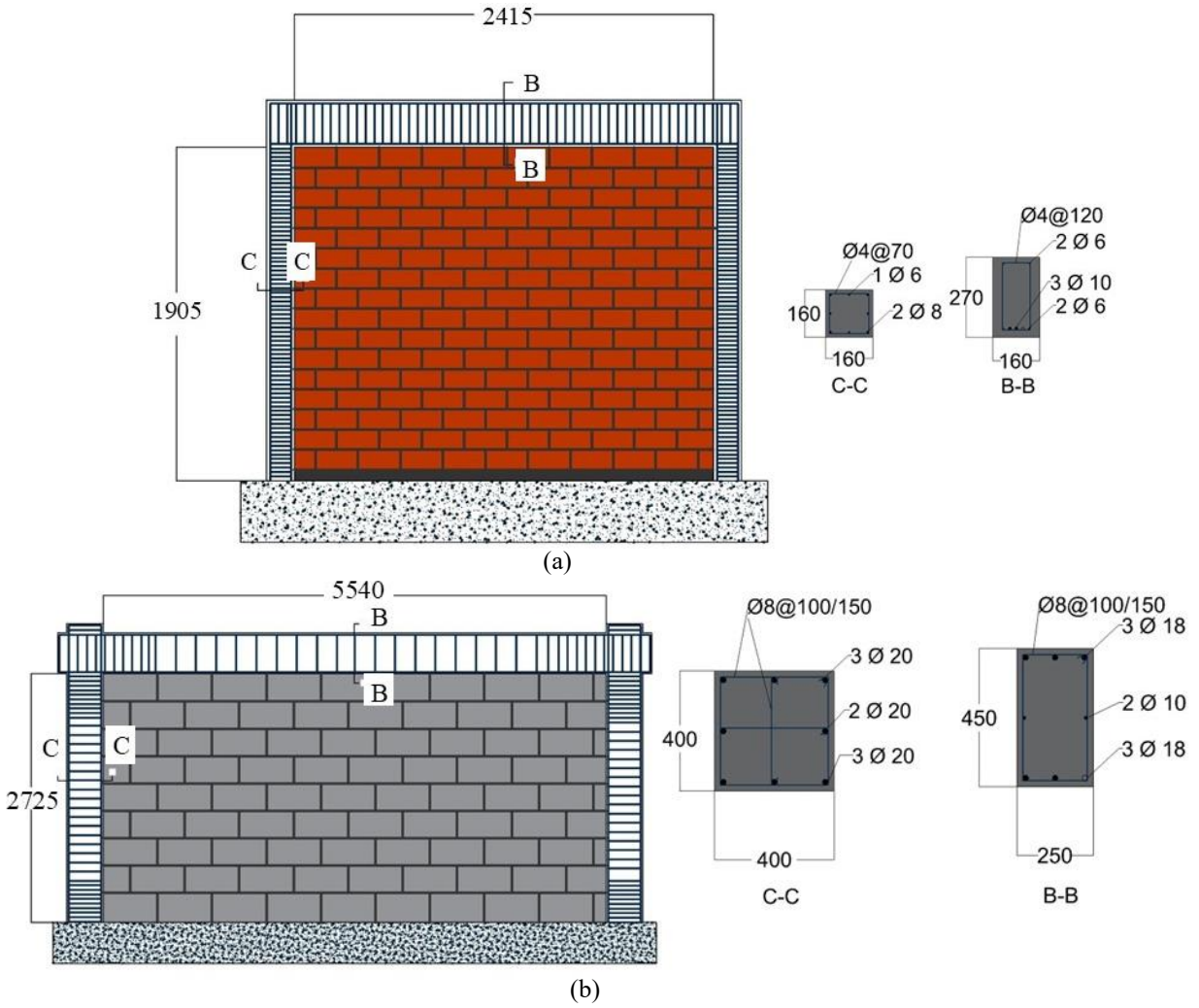

Figure 4: IM-RC frames used to validate the numerical modelling method by (a) Jiang et al [82] and (b) Akhoundi et al [92].

Validation of Numerical IM-RC Model

Two sets of experimental results were used to validate the numerical model developed for analysing the in-plane responses of IM-RC frames. The experimental results were taken from the IM-RC frame testing conducted by Jiang et al., [82] and Akhoundi et al., [92]. The frames tested under in-plane cyclic loading conditions in those studies are shown in Figure 4. The modelling method was validated through simulating these two separate experimental studies (four different IM-RC frames), and then used to analyse various IM-RC frames with different mechanical properties (IM and RC) and geometrical configurations. The numerical models of bare and IM-RC frames tested in those studies were created in OS [39], and the cyclic loading protocols applied were similar to that used in experimental testing. The important IM and RC frame properties used in the models are given in Table 3. Other supplementary parameters computed to assign in the models for validation are given in ***Supplementary data B*** (see the online version).

The IMs used in Jiang et al., [82] were assembled using AAC blocks, where its compressive strength was 3.45 MPa. The IMs used in Akhoundi et al., [92] were constructed using perforated clay blocks with a premix mortar class of M5; and the average compressive strength of the masonry was 1.17 MPa. The longitudinal reinforcement ratio of 0.8% was provided in the columns of RC frames used in Akhoundi et al., [92], whereas one of 2% provided in those tested in Jiang et al [82]. In terms of transverse reinforcement close to critical regions, columns of the frames in Akhoundi et al., [92] and Jiang et al., [82] were provided with 0.2% and 0.4%, respectively. According to the categorisation method outlined in Section 3.1, the IM-RC frames tested in in Akhoundi et al., [92] can be regarded as non-ductile, while those tested in Jiang et al., [82] as ductile. The considerable differences between these two frames in terms of their reinforcement detailing served to validate the numerical modelling across a range of parameters and properties.

Figure 5 shows the experimental and numerically predicted cyclic load-displacement curves of bare and IM-RC frames analysed. A fairly good match between the experimental and numerically predicted cyclic load-displacement curves can be observed. To further substantiate the validation, the critical points (yield, peak and ultimate) in the load-displacement curves (experimental and numerical) were derived and are presented in Table 4. For this purpose, both these set of curves were idealised as outlined in Section 3.2, where an equivalent energy concept was used to derive the idealised curves as per Muguruma et al., [112], and obtain the yield, peak and ultimate points. The initial stiffness was computed from the linear portion of the curves. It can be noted from Table 4 that the errors between the predicted and experimental values (initial stiffness, yield, peak and ultimate load/drift values) are within an acceptable 15% - masonry is a highly variable material, so deviation in the predictions up to 15% could be considered as acceptable, e.g. EN 1996-1-1 [50]. Given the variations in the experimental set-ups used, slight deviations in the shapes of hysteresis curves predicted can be noted; this is inevitable, with different structural elements and their interactions involved in the analyses.

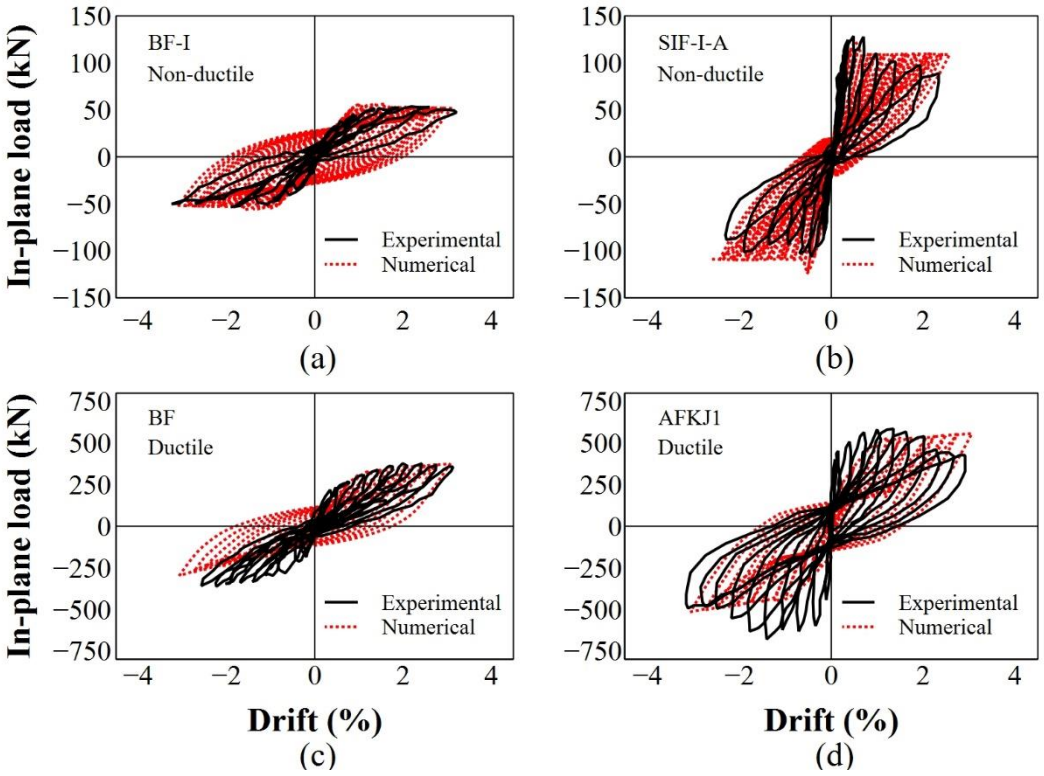

Figure 5: Experimental vs. numerical in-plane cyclic responses of bare and IM-RC frames: (a) Akhoundi et al [92]: Bare frame (b) Akhoundi et al [92]: IM-RC frame, (c) Jiang et al [82]: Bare frame, and (d) Jiang at al [82]: IM-RC frame.

Table 3: Mechanical parameters of IM and RC used in the numerical model.

	Parameters	Akhoundi et al [92]	Jiang et al [82]
Concrete	Compressive strength of concrete (f_c)	25 MPa	28.5 MPa
	Strain corresponding to the peak strength of concrete (ε_c)	0.029	0.022
	Elastic modulus of concrete (E_c)	27.42 GPa	28.8 GPa
	Tensile strength of the concrete (f_{ct})	3.1 MPa	3.31 MPa
	Strain corresponding to the concrete tensile failure (ε_t)	0.00011	0.00012
Steel	Yield strength of the reinforcement bar (f_{st})	400 MPa	450 MPa
	Elastic modulus of reinforcement bar (E_{st})	210 GPa	200 GPa
IM	Peak compressive strength of masonry (f_m)	1.2 MPa	3.5 MPa
	Strain corresponding to the peak strength of masonry (ε_{cm})	0.003	0.0022
	Ultimate strength of masonry (f_{mu})	0.96 MPa	2.8 MPa
	Strain corresponding to the ultimate stress of masonry (ε_{mu})	0.003	0.003

Overall, it can be said that the developed numerical modelling is appropriate and effective for analysing different types of IM-RC frames. This validated numerical modelling technique was used to extend analyse the IM-RC configurations missing in the database created. Those details are given in next section.

ANALYSES OF IM-RC FRAMES

Given that the numerical modelling method established to simulate the behaviour has shown its ability to predict the in-plane cyclic responses of different IM-RC frames, it was used to analyse the IM-RC frame configurations that are not explicitly tested in the past experimental studies, such configurations already highlighted in Section 3.2 and Figure 1. The configurations highlighted as "Gaps" (in Figure. 1) were numerically analysed. In total, 320 IM-RC frame models were created and analysed to fill the gaps in the experimental database. An alpha numeric nomenclature system was assigned to each IM-RC case analysed. The nomenclature has five sets of connotations, the generic form can be given as f_m-f_c-h/l-ρ_l-*ND/D*, which is according to the categorisation made in in Section 3.2. For an example, 4-30-0.75-0.8-ND refers to a IM-RC frame analysed with 4 MPa masonry strength and 30 MPa concrete strength in columns. The aspect ratio of the IM is 0.75 (i.e. 3 m high and 4 m length) and longitudinal reinforcement percentage provided is 0.8%, hence it is a non-ductile frame. The data of numerically analysed IM-RC frames with their nomenclatures are given in ***Supplementary data C*** (see the online version).

Table 5 provides the variables considered in the IM-RC frame configurations analysed, which are based on the gaps identified in Section 3.2. To analyse different IM strengths according to the categorisation specified, masonry compressive strengths ranging 2 MPa to 20 MPa were used. Concrete strengths of 15 MPa, 25 MPa, 30 MPa and 40 MPa were considered.

Table 4: Comparison of experimental and numerical values in the idealized load-displacement curves.

Parameters		Akhoundi et al. [92]	Akhoundi et al. [92]	Jiang et al. [82]	Jiang et al. [82]
Frame notation		Bare: BF-I	IM-RC: SIF-I-A	Bare frame: BF	IM-RC: AFKJ1
Initial Stiffness (kN/m)	Experimental	2417.17	19385.37	21489.5	47027.00
	Numerical	2719.68	17172.08	21487.5	41531.43
	Error (%)	12.52	11.42	0.0	11.69
Yield force (kN)	Experimental	42.90	102.82	306.87	470.27
	Numerical	44.94	101.59	306.87	454.25
	Error (%)	4.78	1.20	0.0	3.41
Drift at yield (δ_y)	Experimental	0.87	0.26	1.02	0.32
	Numerical	0.81	0.29	1.02	0.35
	Error (%)	6.89	11.54	0.0	9.38
Peak force ((kN)	Experimental	53.62	128.52	361.83	585.26
	Numerical	56.17	126.99	355.73	598.75
	Error (%)	4.76	1.19	1.69	2.30
Drift at peak (δ_p)	Experimental	2.00	0.49	1.84	1.35
	Numerical	1.84	0.55	1.83	1.33
	Error (%)	8.00	12.24	0.54	1.48
Ultimate force /(kN)	Experimental	45.24	88.77	331.3	428.99
	Numerical	48.58	95.24	374.43	623.64
	Error (%)	7.38	7.29	13.02	45.37
Drift at ultimate (δ_u)	Experimental	3.21	2.34	3.13	2.82
	Numerical	3.09	2.55	3.06	3.06
	Error (%)	3.74	8.97	2.24	8.51

Table 5: Summary of IM-RC frame cases analysed using numerical method.

Gap	f_m (MPa)	f_c (MPa)	h/l	ρ_v (%)
1	2,4	15, 25, 30, 40	1.5, 2.0	1.31, 2.05
2	2,4		1.5, 2.0	1.79, 2.79
3	7.5,10,12.5		0.75, 1.0	0.5, 0.75
4	7.5,10,12.5		0.75, 1.0	1.79, 2.79
5	7.5,10,12.5		1.5, 2.0	1.31, 2.05
6	7.5,10,12.5		1.5, 2.0	1.79, 2.79
7	17.5,20		0.75, 1.0	1.31, 2.05
8	17.5,20		1.5, 2.0	1.31, 2.05

For $h/l \leq 1$, ratios of 0.6, 0.75 and 1.0, were considered, and for $h/l > 1$, ratios of 1.5 and 2.0 were analysed. The height of the IM, i.e. h, was maintained at 3 m in all cases. To simulate the non-ductile and ductile frame configurations in combinations with above method variables, different RC column sections, as shown in Figure 6, were considered. The non-ductile column configurations were derived based on the commonly used reinforcement detailing in Sri Lanka for low-rise IM-RC buildings. For example, typical IM-RC school buildings in Sri Lanka have these types of reinforcement detailing - more details on the typical reinforcement detailing in Sri Lankan schools can be referred to in Del Zoppo et al., [113]. The ductile columns configurations were decided on by upgrading those existing column configurations to be compliant to the seismic demand in a Sri Lankan context. Therefore, all the missing configurations in the experimental database have been incorporated and simulated.

In-Plane Load-Drift Responses Derived

The in-plane load-drift responses of IM-RC frames obtained through the experimental database (explained in Section 3.1) and numerical analyses are given in this section. Although the IM-RC frames were categorised as per masonry strengths, concrete strengths, aspect ratios, and reinforcement detailing, the load-drift responses are presented according to IM strengths (low, medium and high), and reinforcement detailing (i.e. non-ductile and ductile). The in-plane load-drift responses of non-ductile and ductile IM-RC frames are given in Figures 7 and 8, respectively. The experimental and numerical in-plane load-drift responses are both presented separately and then combined; and categorized according to both IM strengths and reinforcement detailing (i.e. non-ductile and ductile). The fragility functions for IM-RC frames were also established based on the same categorisations.

Some general inferences can be drawn from the load-drift responses obtained in experimental and numerical studies. It can be said that the increase of IM strength tends to increase the in-plane load carrying capacities and reduce the drift capacities of the frames. Changes in the concrete strength used in RC elements did not greatly affected the in-plane load-drift response of the IM-RC frame analysed. Obviously, the ductile IM-RC frames have shown greater load and drift capacities than the non-ductile IM-RC frames.

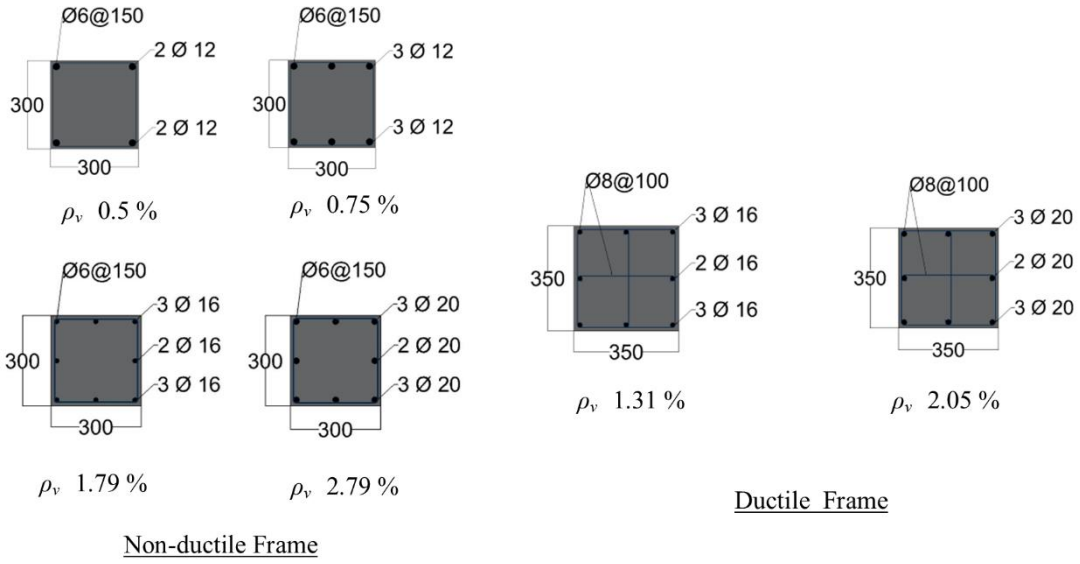

Figure 6: Non-ductile and ductile column configurations used in numerical analyses.

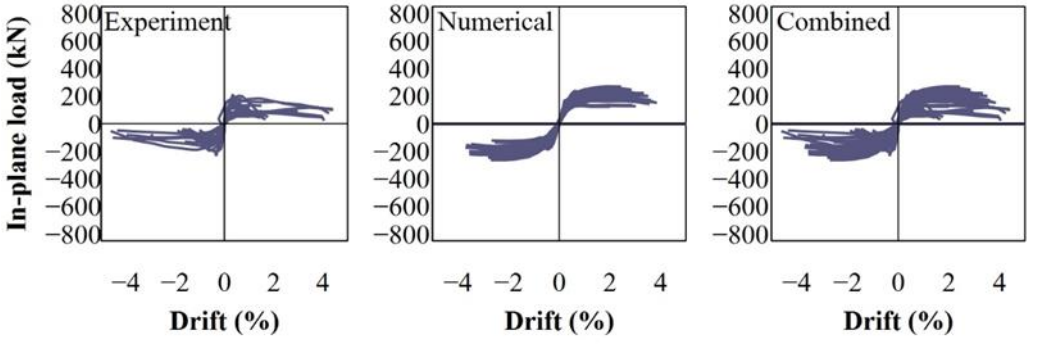

(a)

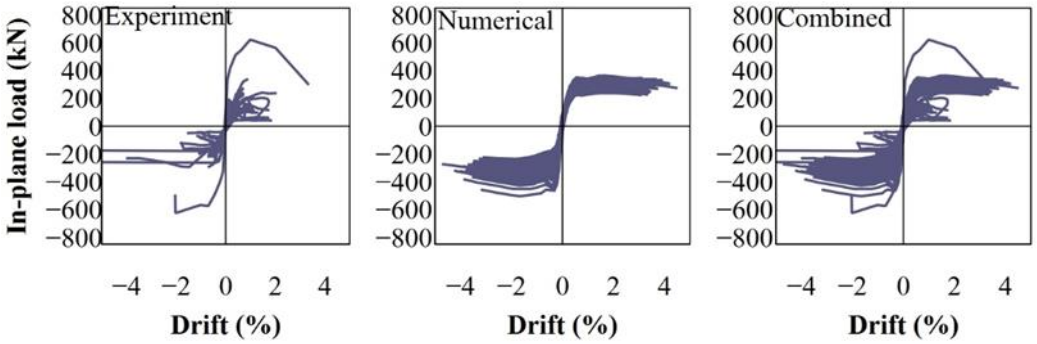

(b)

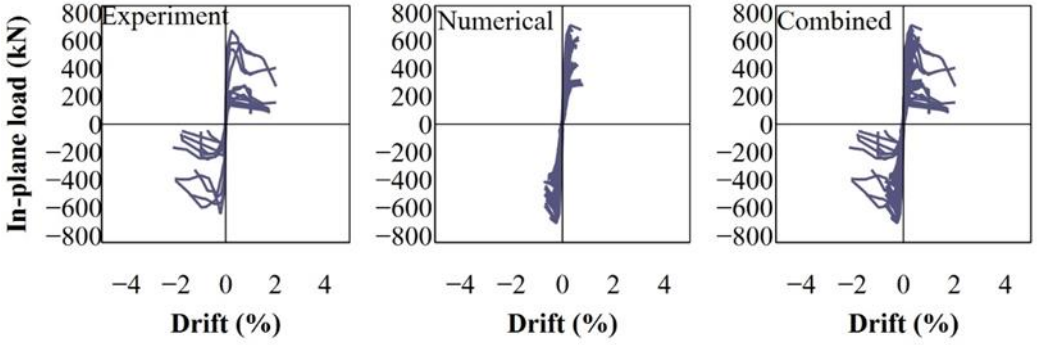

(c)

Figure 7: Cluster of curves of non-ductile IM-RC frames under in-plane loading (a) fm ≤ 5 MPa, (b) 5 MPa < fm ≤ 15 MPa and (c) fm > 15 MPa.

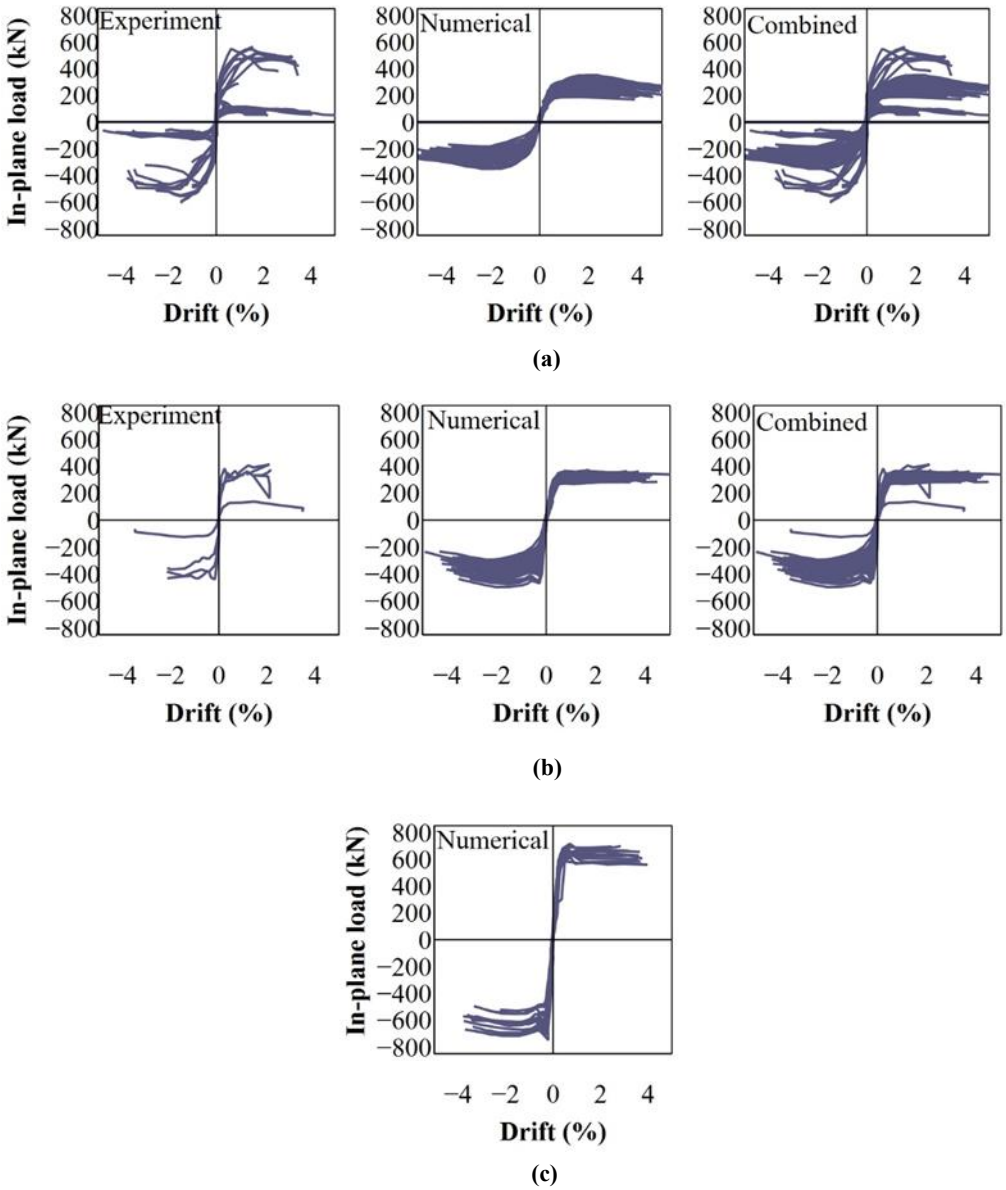

Figure 8: Cluster of curves of ductile IM-RC frames under in-plane loading (a) fm ≤ 5 MPa, (b) 5 MPa < fm ≤ 15 MPa and (c) fm > 15 MPa.

The aspect ratios of the IMs had mixed responses in the in-plane load-drift capacities of the frames analysed; IM-RC frames with *h/l* ratios more than 1.0 tended to show more drift capacities than the (more squat) frames with *h/l* less than 1.0. In terms of load carrying capacities, the IM-RC frames with *h/l* ratios less than 1.0 showed higher capacities than the frames with *h/l* greater than 1.0. This phenomenon is because the lengths of the IMs are greater for *h/l* ratios less than 1.0. In addition, the non-ductile RC frames with high strength IMs (i.e. > 15 MPa) have shown the lowest drift capacities among the cases analysed (see Figure 7(c)); this is due to the high thrust forces excreted by IMs to non-ductile RC frames, thus causing early failure of the frames. In Figure 8(c), only the in-plane load-drift responses obtained through numerical analyses are presented, since no experimental test data is available under the category of ductile RC frames with high strength IMs. However, it has to be mentioned that these observations are generic in nature, as the in-plane behaviour of IM-RC frames is influenced by multiple interrelated factors. Hence, the experimental and numerical cases analysed have been clustered to develop fragility functions.

Development of Fragility Functions

To establish the fragility curves, drift levels attained (correspond to each damage state defined) in each IM-RC frame configurations analysed (both experimentally and numerically) were retrieved from the load-drift responses obtained.

Using the drift data gathered, the fragility functions were developed using the lognormal distribution function provided in FEMA P-58 [114], which is given in Eq (3). Here, $F_i(\delta)$ is the conditional probability of reaching a specified damage state (DS) at a given in-plane drift ratio. Φ, $\theta_{i,ds}$ and β_{ds} are the standard normal cumulative distribution function, the median value of the probability distribution, and logarithmic standard deviation, respectively. The values of $\theta_{i,ds}$ and β_{ds} were determined from Eqs (4) and (5), respectively.

$$F_i(\delta) = \Phi\left(\frac{\ln(\delta_i/\theta_{i,ds})}{\beta_{ds}}\right) \quad (3)$$

$$\theta_{i,ds} = e^{(1/M \sum_{i=1}^{M} ln\delta_i)} \quad (4)$$

$$\beta_{ds} = \sqrt{\beta_{ds,r}^2 + \beta_{dsu}^2} \quad (5)$$

$\beta_{ds,r}$ is defined in Eq (6), and M accounts for the number of datasets used in the analysis (i.e. the number of IM-RC frame cases used to derive the fragility functions). According to FEMA P-58 [114], $\beta_{ds,u}$ can be assumed equal to 0.10 or 0.25 for databases of good and deficient qualities respectively. Consequently, in this research, $\beta_{ds,u}$ was assumed as 0.10.

$$\beta_{ds,r} = \sqrt{\left(\frac{1}{M-1}\sum_{i=1}^{M}\left(\ln\left(\frac{\delta_i}{\theta_{i,ds}}\right)\right)^2\right)^2} \quad (6)$$

The established fragility functions are presented in Figures 9 and 10, for the non-ductile and ductile IM-RC frames, respectively. The fragility curves are categorised according to the strength of IM used in frames. Since the fragility curves were developed from combined experimental and numerical data, the fragility curve obtained based only on experimental or numerical analyses are also presented for comparisons. Only in Figure 10(c), for the ductile RC frames with high strength IM combinations, no experimental data is available, hence the fragility functions were developed based only on the numerical data generated. Some of the fragility curves derived display as almost vertical lines. This is because the IM strength and RC frame types (ductile and non-ductile) greatly influence the in-plane behaviour of IM-RC frame, and they are already categorised as (a) to (c) in Figures 9 and 10. Hence, the near-verticality that arises in the numerical curves are due to limited variability in the IM-RC frame cases analysed within a given sub-category, especially because the numerical datasets are used only for filling the parameter gaps in the experimental ones. Note in particular that Figure 9c is for high strength masonry and non-ductile IM-RC frames, which have shown brittle failure (with limited post-peak response, see Figure 7c) compared to other cases analysed. The high strength IM creates a relatively high thrust force, causing the IM and RC frame to fail in very close sequence. The drift levels derived and the corresponding fragility curves tend to be vertical and close to each other. Also, it has to be emphasised that the numerical and experimental fragility curves produced should not be compared directly (though they are categorised according to IM strengths), as they are derived from different sets (aspect ratio, concrete strength and reinforcement detailing) of IM-RC frame configurations

From the fragility functions established, it is apparent that the non-ductile RC frames are more vulnerable than the ductile RC frames for all the different combinations of IM strengths used. Also comparisons within the non-ductile or ductile IM-RC frame configurations functions reveal that an increase in IM strength (i.e. compressive strength) tends to increase the vulnerability of the frames under in-plane loading, as the drift levels attained at each damage state tend to reduce with the increase in IM strength. This phenomenon can be clearly seen from the fragility curves of non-ductile RC frames; whereas the ductile RC frame cases showed rather minimal influence of the masonry strength properties to the in-plane response, particularly for DS3 and DS4 curves. However, the deviations observed between the experimental and numerical sets of fragility curves (for similar categorisation) are due to the resulting diversity of the IM-RC configurations analysed, since the numerical datasets were specifically created to supplement missing parameter gaps in the experimental ones.

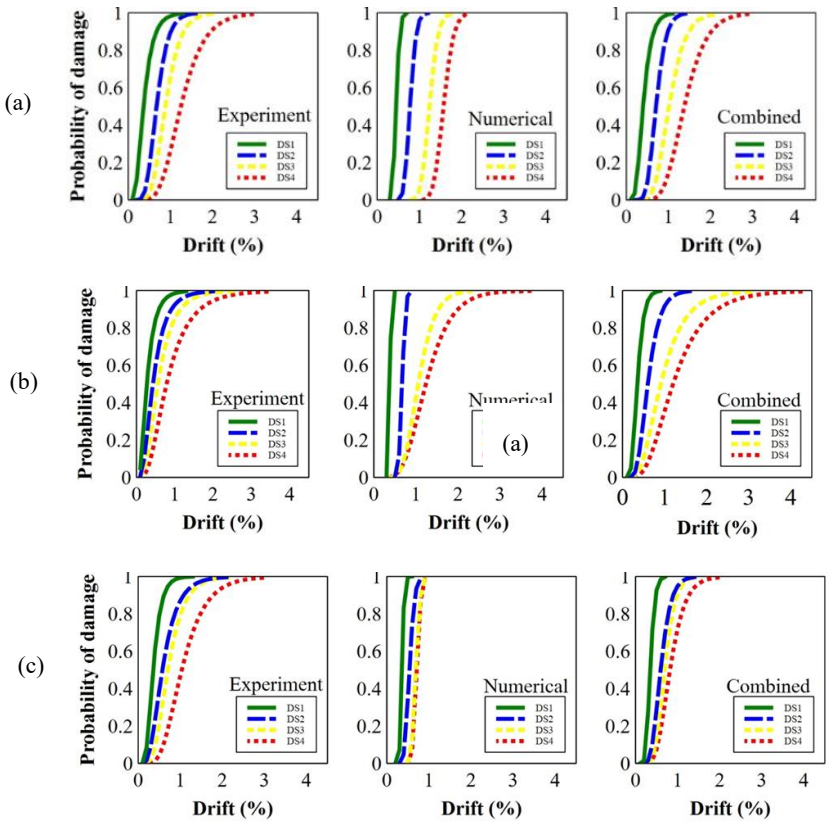

Figure 9: Fragility functions of non-ductile IM-RC frames under in-plane loading (a) fm ≤ 5 MPa, (b) 5 MPa < fm ≤ 15 MPa and (c) fm > 15 MPa.

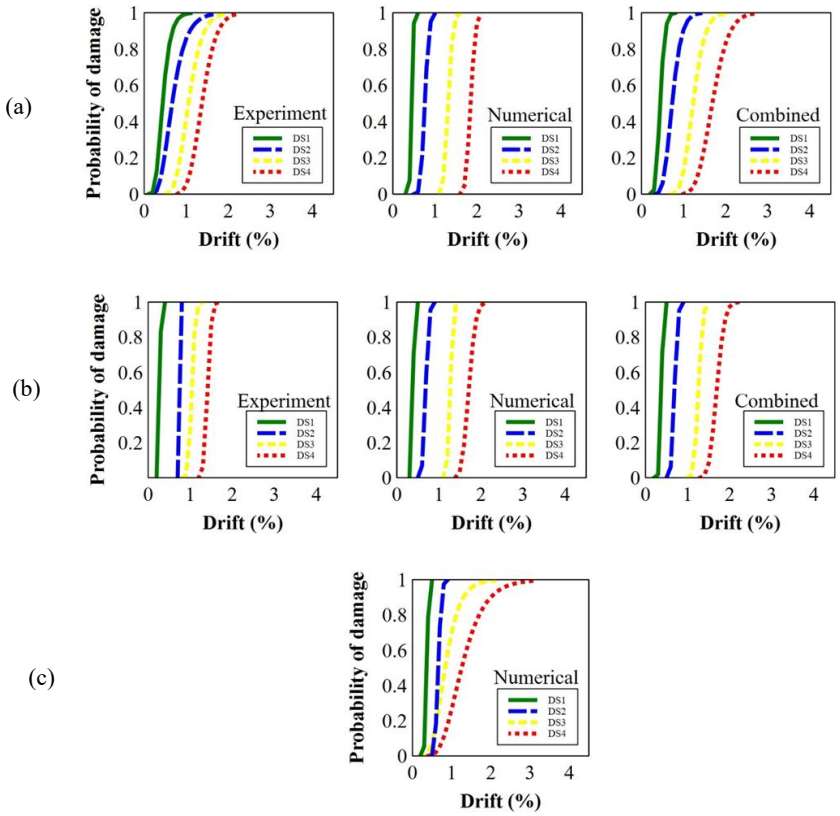

Figure 10: Fragility functions of ductile IM-RC frames under in-plane loading (a) fm ≤ 5 MPa, (b) 5 MPa < fm ≤ 15 MPa and (c) fm > 15 MPa.

To properly compare the performance of the IM-RC configurations s analysed, $\theta_{i,ds}$ and $\beta_{i,ds}$ values determined for each fragility curve are given in Table 6. The dispersion in the fragility curves (i.e. $\beta_{i,ds}$values reported in Table 6) are inevitable, as the fragility functions were derived from the diverse sets of IM-RC configurations analysed. The $\theta_{i,ds}$ values obtained clearly show that the increase in IM strength reduces the drift limits of the IM-RC frame configurations analysed, in particular when high strength IMs (> 15 MPa) are used with non-ductile frames. For example, a low strength IM with a non-ductile RC frame reached DS4 at 2.09% drift level (median), whereas the high strength IM with the non-ductile RC frame reached the same DS4 at only 0.63% drift (median).

The fragility functions established in this study have clearly shown the differing vulnerabilities of the different types of IM-RC configurations, with the functions developed systematically using both experimental and numerical datasets that encompass different IM (strength class) and RC frame (detailing) configurations. The previous studies have only used experimental data to develop the fragility functions. However, it has been shown in Section 3 that the experimental data of IM-RC frames tested under in-plane loading conditions are limited, with several combinations of IM-RC configurations not experimentally tested; thus causing the fragility functions provided in those studies to be limited in coverage. Therefore, the fragility functions generated in this study have expanded the coverage, allowing them to be used rationally to assess the vulnerability and compute potential losses corresponding to the entire range of IM-RC frame categories that exist in real practice.

SUMMARY AND CONCLUSIONS

Fragility functions for fully filled IM-RC frames under in-plane loading conditions have been established using a hybrid approach. Analyses of experimental studies conducted on testing single storey-single bay IM-RC frames under in-plane loading conditions showed that the in-plane behaviour of certain IM-RC frame configurations are not explicitly investigated. To fill these gaps in the experimental knowledge on the in-plane behaviour of IM-RC frames, a numerical method of analysing single storey-single bay IM-RC frames was developed using OS [39], and the in-plane behaviour of those configurations analysed. Appropriate constitutive laws that incorporate the failure of concrete, yielding of reinforcement, bond slip and shear failure of RC sections were integrated in the modelling method adopted. The IM in the numerical modelling method was represented using double strut diagonals. The capability of the numerical modelling method was proved by validating it against some of the experimental studies on IM-RC frames under in-plane cyclic loading conditions, and good agreements between the numerical predictions on the experimental results are demonstrated. The validated modelling method was used to analyse the IM-RC frame configurations that have not been explicitly tested in experimental studies. In total, 320 numerical IM-RC frame models have been created with different IM and RC configurations and analysed under in-plane cyclic loading conditions. The experimental and numerical datasets generated were used to establish the fragility functions.

Four damage states were established accounting for the failure evolution of IM-RC frames under in-plane loading conditions, reflecting the damage to IM and RC frame (repairable and non-repairable).

Table 6: Statistical parameters of the fragility functions.

Frame type	IM strength	Experimental			Numerical			Combined		
		Damage states	$\theta_{i,ds}$	$\beta_{i,ds}$	Damage states	$\theta_{i,ds}$	$\beta_{i,ds}$	Damage states	$\theta_{i,ds}$	$\beta_{i,ds}$
Non-ductile	Low	DS1	0.09	0.48	DS1	0.16	0.15	DS1	0.12	0.38
		DS2	0.40	0.32	DS2	0.56	0.14	DS2	0.45	0.26
		DS3	0.67	0.29	DS3	1.64	0.13	DS3	1.04	0.29
		DS4	0.80	0.27	DS4	2.84	0.12	DS4	2.09	0.30
	Medium	DS1	0.05	0.60	DS1	0.11	0.07	DS1	0.09	0.33
		DS2	0.14	0.59	DS2	0.40	0.09	DS2	0.31	0.37
		DS3	0.26	0.55	DS3	1.13	0.29	DS3	0.81	0.48
		DS4	0.58	0.55	DS4	1.25	0.35	DS4	1.53	0.49
	High	DS1	0.09	0.42	DS1	1.95	0.11	DS1	0.09	0.25
		DS2	0.28	0.49	DS2	0.24	0.18	DS2	0.30	0.32
		DS3	0.45	0.43	DS3	0.42	0.12	DS3	0.42	0.28
		DS4	1.08	0.42	DS4	0.45	0.11	DS4	0.63	0.34
Ductile	Low	DS1	0.15	0.33	DS1	0.15	0.07	DS1	0.15	0.19
		DS2	0.39	0.38	DS2	0.53	0.10	DS2	0.48	0.24
		DS3	1.13	0.24	DS3	1.88	0.07	DS3	1.60	0.18
		DS4	2.08	0.19	DS4	4.11	0.05	DS4	3.32	0.18
	Medium	DS1	0.05	0.06	DS1	0.11	0.08	DS1	0.11	0.11
		DS2	0.51	0.01	DS2	0.42	0.09	DS2	0.42	0.09
		DS3	1.09	0.06	DS3	1.71	0.04	DS3	1.69	0.06
		DS4	2.21	0.05	DS4	3.39	0.08	DS4	3.36	0.09
	High	DS1	-	-	DS1	0.08	0.12	DS1	-	-
		DS2	-	-	DS2	0.37	0.11	DS2	-	-
		DS3	-	-	DS3	0.65	0.32	DS3	-	-
		DS4	-	-	DS4	1.70	0.37	DS4	-	-

The fragility functions established have been categorised according to the type of RC frame and IM, where RC frame configurations are subdivided into non-ductile and ductile, and the IM types sub-categorised into low (≤ 5 MPa), medium (> 5 MPa & ≤ 15 MPa) and high (> 15 MPa) strength masonry assemblages. The fragility curves developed clearly show that the non-ductile IM-RC frames are more vulnerable than the ductile IM-RC ones. Comparisons of fragility curves derived at DS4 (i.e. collapse/ultimate) indicate that the non-ductile frames are 60-110% more vulnerable than the ductile ones. However, uncertainties are associated in the fragility curves derived, as could be noted from the $\beta_{i,ds}$ values reported in Table 6.

Also, an increase in IM strength tends to increase the vulnerability of the IM-RC frame, as the high strength IMs are likely to increase diagonal thrust actions on the surrounding RC frame when subjected to in-plane loading, leading to early failure of such frames. This phenomenon can be clearly noted from the fragility curves of non-ductile RC frames; whereas the ductile RC frame cases showed rather minimal influence of the masonry strength properties to the in-plane response, particularly for DS3 and DS4 curves. This could be due to the dominant behaviour of the ductile RC frame over the IM thrust action, as the sizes of RC elements in ductile frames are greater; adequate shear capacities are also provided through stirrups, hence IM induced shear forces are taken care of.

This highlights the importance of designing ductile RC frames when using IM walls in seismic regions. It is important to appreciate however that the increases in IM strength would also increase the base shear capacity of the IM-RC frame. Hence a trade-off is needed when designing IM-RC frames using strength and displacement based approaches.

The fragility curves reported in this study can be regarded as holistic, as they have been developed using diverse experimental and numerical datasets, based on the damage sequences observed. Hence, they could be used rationally to assess seismic vulnerability and compute losses associated with the IM-RC frame configurations analysed in this study. However, it has to be highlighted that the fragility curves developed are limited to single storey-single bay fully filled IM-RC frame configurations, and in-plane loading conditions. Further studies are needed in the future to extend fragility functions developed to other IM-RC frame configurations such as those with IM openings and multiple storeys; and also to multi-directional loading conditions.

ACKNOWLEDGEMENTS

Authors like to thank the Department of Civil Engineering, University of Moratuwa for the technical and administrative assistance provided for this research study

REFERENCES

1 Alwashali H, Islam MS, Sen D, Monical J and Maeda M (2020). "Seismic capacity of RC frame buildings with masonry infill damaged by past earthquakes". *Bulletin of the New Zealand Society for Earthquake Engineering,* **53**(1): 13-21. https://doi.org/10.5459/bnzsee.53.1.13-21

2 Giaretton M, Dizhur D, da Porto F and Ingham JM (2016). "Seismic assessment and improvement of unreinforced stone masonry buildings: literature review and application to New Zealand". *Bulletin of the New Zealand Society for Earthquake Engineering,* **49**(2): 148-174. https://doi.org/10.5459/bnzsee.49.2.148-174

3 Cavaleri L, Di Trapani F, Asteris PG and Sarhosis V (2017). "Influence of column shear failure on pushover based assessment of masonry infilled reinforced concrete framed structures: A case study". *Soil Dynamics and Earthquake Engineering,* **100**: 98-112. https://doi.org/10.1016/j.soildyn.2017.05.032

4 Asteris PG, Cotsovos DM, Chrysostomou CZ, Mohebkhah A and Al-Chaar GK (2013). "Mathematical micromodeling of infilled frames: State of the art". *Engineering Structures,* **56**: 1905-1921. https://doi.org/10.1016/j.engstruct.2013.08.010

5 Perrone D, Brunesi E, Filiatrault A and Nascimbene R (2020). "Probabilistic estimation of floor response spectra in masonry infilled reinforced concrete building portfolio". *Engineering Structures,* **202**: 109842. https://doi.org/10.1016/j.engstruct.2019.109842

6 Donà M, Minotto M, Verlato N and da Porto F (2022). "A new macro-model to analyse the combined in-plane/out-of-plane behaviour of unreinforced and strengthened infill walls". *Engineering Structures,* **250**: 113487. https://doi.org/10.1016/j.engstruct.2021.113487

7 Sarno L Di and Wu JR (2021). "Fragility assessment of existing low-rise steel moment-resisting frames with masonry infills under mainshock-aftershock earthquake sequences". *Bulletin of Earthquake Engineering,* **19**(6): 2483-2504. https://doi.org/10.1007/s10518-021-01080-6

8 Gautam D, Adhikari R and Rupakhety R (2015). "Seismic fragility of structural and non-structural elements of Nepali RC buildings". *Engineering Structures,* **232**: 111879. https://doi.org/10.1016/j.engstruct.2021.111879

9 Ricci P, De Risi MT, Verderame GM and Manfredi G (2013). "Influence of infill distribution and design typology on seismic performance of low-and mid-rise RC buildings". *Bulletin of Earthquake Engineering,* **11**: 1585-1616. https://doi.org/10.1007/s10518-013-9453-4

10 Perrone D, Leone M and Aiello MA (2017) "Non-linear behaviour of masonry infilled RC frames: Influence of masonry mechanical properties". *Engineering Structures,* **150**: 875-891. https://doi.org/10.1016/j.engstruct.2017.08.001

11 Barbosa AR, Fahnestock LA, Fick DR, Gautam D, Soti R, Wood R, Moaveni B, Stavridis A, Olsen MJ and Rodrigues H (2017). "Performance of medium-to-high rise reinforced concrete frame buildings with masonry infill in the 2015 Gorkha, Nepal, earthquake". *Earthquake Spectra,* **33**: 197-218. https://doi.org/10.1193/051017eqs087m

12 Furtado A, Rodrigues H and Arêde A (2015). "Modelling of masonry infill walls participation in the seismic behaviour of RC buildings using OpenSees". *International Journal of Advanced Structural Engineering (IJASE),* **7**: 117-127. https://doi.org/10.1007/s40091-015-0086-5

13 Furtado A, Rodrigues H, Arêde A and Varum H (2020). "Experimental tests on strengthening strategies for masonry infill walls: A literature review". *Construction and Building Materials,* **263**: 120520. https://doi.org/10.1016/j.conbuildmat.2020.120520

14 Pradhan B, Zizzo M, Sarhosis V and Cavaleri L (2021). "Out-of-plane behaviour of unreinforced masonry infill walls: Review of the experimental studies and analysis of the influencing parameters". *Structures*, **33:** 4387-4406. https://doi.org/10.1016/j.istruc.2021.07.038

15 F Furtado A, Rodrigues H, Arêde A and Varum H (2018). "Out-of-plane behavior of masonry infilled RC frames based on the experimental tests available: A systematic review". *Construction and Building Materials,* **168**: 831-848. https://doi.org/10.1016/j.conbuildmat.2018.02.129

16 Huang H and Burton HV (2020). "A database of test results from steel and reinforced concrete infilled frame experiments". *Earthquake Spectra,* **36**(3): 1525-1548. https://doi.org/10.1177/8755293019899950

17 Tarque N, Candido L, Camata G and Spacone E (2015). "Masonry infilled frame structures: State-of-the-art review of numerical modelling". *Engineering Structures,* **8**(1): 225–51. https://doi.org/10.12989/eas.2015.8.1.225

18 Trapani F Di (2021). "A novel data-driven force–displacement macro-model for nonlinear analysis of infilled frames: development, validation and reliability comparison". *Bulletin of Earthquake Engineering,* **19**: 6157-6186. https://doi.org/10.1007/s10518-021-01211-z

19 Stavridis A, Koutromanos I and Shing PB (2012). "Shake-table tests of a three-story reinforced concrete frame with masonry infill walls". *Earthquake Engineering and Structural Dynamics,* **41**(6): 1089–108. https://doi.org/10.1002/eqe.1174

20 Gong M, Zuo Z, Wang X, Lu X and Xie L (2019). "Comparing seismic performances of pilotis and bare RC frame structures by shaking table tests". *Engineering Structures,* **199**: 109442. https://doi.org/10.1016/j.engstruct.2019.109442

21 Guljaš I, Penava D, Laughery L and Pujol S (2020). "Dynamic tests of a large-scale three-story RC structure with masonry infill walls". *Journal of Earthquake Engineering,* **24**(11): 1675-1703. https://doi.org/10.1080/13632469.2018.1499203

22 Cavaleri L and Trapani F Di (2014). "Cyclic response of masonry infilled RC frames: Experimental results and simplified modeling". *Soil Dynamics and Earthquake Engineering,* **65**: 224-242. https://doi.org/10.1016/j.soildyn.2014.06.016

23 Hossameldeen M and Romão X (2020). "Analysis of the performance of strut models to simulate the seismic behaviour of masonry infills in partially infilled RC frames". *Engineering Structures,* **222**: 111124. https://doi.org/10.1016/j.engstruct.2020.111124

24 Morandi P, Hak S and Magenes G (2018). "Performance-based interpretation of in-plane cyclic tests on RC frames with strong masonry infills". *Engineering Structures,* **156**: 503-521. https://doi.org/10.1016/j.engstruct.2017.11.058

25 Sassun K, Sullivan TJ, Morandi P and Cardone D (2016). "Characterising the in-plane seismic performance of infill masonry". *Bulletin of the New Zealand Society for Earthquake Engineering,* **49**(1): 98-115. https://doi.org/10.5459/bnzsee.49.1.98-115

26 Liberatore L, Noto F, Mollaioli F and Franchin P (2018). "In-plane response of masonry infill walls: Comprehensive experimentally-based equivalent strut model for deterministic and probabilistic analysis". *Engineering Structures,* **167**: 533-548. https://doi.org/10.1016/j.engstruct.2018.04.057

27 Noh NM, Liberatore L, Mollaioli F and Tesfamariam S (2017). "Modelling of masonry infilled RC frames subjected to cyclic loads: State of the art review and modelling with OpenSees". *Engineering Structures,* **150**: 599-621. https://doi.org/10.1016/j.engstruct.2017.07.002

28 Romano F, Alam MS, Zucconi M, Faggella M, Barbosa AR and Ferracuti B (2021). "Seismic demand model class uncertainty in seismic loss analysis for a code-designed URM infilled RC frame building". *Bulletin of Earthquake Engineering,* **19**(1): 429-462. https://doi.org/10.1007/s10518-020-00994-x

29 De Risi MT, Del Gaudio C, Ricci P and Verderame GM (2018). "In-plane behaviour and damage assessment of masonry infills with hollow clay bricks in RC frames". *Engineering Structures,* **168**: 257-275. https://doi.org/10.1016/j.engstruct.2018.04.065

30 Huang H, Burton HV and Sattar S (2020). "Development and utilization of a database of infilled frame experiments for numerical modeling". *Journal of Structural Engineering,* **146**(6): 04020079. https://doi.org/10.1061/(ASCE)ST.1943-541X.0002608

31 Haindl M, Burton HV and Sattar S (2024). "Quantification of equivalent strut modeling uncertainty and its effects on the seismic performance of masonry infilled reinforced concrete frames". *Journal of Earthquake Engineering,* **28**(1): 41-61. https://doi.org/10.1080/13632469.2023.2171509

32 Srechai J, Leelataviwat S, Wararuksajja W and Limkatanyu S (2022). "Multi-strut and empirical formula-based macro modeling for masonry infilled RC frames". *Engineering Structures,* **266**: 114559. https://doi.org/10.1016/j.engstruct.2022.114559

33 Sirotti S, Pelliciari M, Trapani F Di, Briseghella B, Marano GC, Nuti C and Tarantino AM (2021). "Development and validation of new Bouc–Wen data-driven hysteresis model for masonry infilled RC frames". *Journal of Engineering Mechanics,* **147**(11): 04021092. https://doi.org/10.1061/(ASCE)EM.1943-7889.0002001

34 Mucedero G, Perrone D, Brunesi E and Monteiro R (2020). "Numerical modelling and validation of the response of masonry infilled RC frames using experimental testing results". *Buildings,* **10**(10): 182. https://doi.org/10.3390/buildings10100182

35 Cardone D and Perrone G (2015). "Developing fragility curves and loss functions for masonry infill walls". *Earthquakes and Structures,* **9**(1): 257-279. http://dx.doi.org/10.12989/eas.2015.9.1.000

36 Chiozzi A and Miranda E (2017). "Fragility functions for masonry infill walls with in-plane loading". *Earthquake Engineering and Structural Dynamics,* **46**(15): 2831-2850. **https://doi.org/10.1002/eqe.2934**

37 Del Gaudio C, De Risi MT, Ricci P and Verderame GM (2019). "Empirical drift-fragility functions and loss estimation for infills in reinforced concrete frames under seismic loading". *Bulletin of Earthquake Engineering,* **17**: 1285-1330. https://doi.org/10.1007/s10518-018-0501-y

38 Xie X, Zhang L and Qu Z (2022). "A critical review of methods for determining the damage states for the in-plane fragility of masonry infill walls". *Journal of Earthquake Engineering,* **26**(9): 4523-4544. https://doi.org/10.1080/13632469.2020.1835749

39 McKenna F, Fenves GL, and Scott MH (2006). "*OpenSees: Open System for Earthquake Engineering Simulation*". Pacific Earthquake Engineering Research Center, UC Berkeley, CA.

40 American Society of Civil Engineers (2017). "*Seismic Evaluation and Retrofit of Existing Buildings*". American Society of Civil Engineers, USA.

41 CEN (2004). "*EN 1998-1:2004: European Standard Eurocode 8: Design of Structures for Earthquake Resistance*". Comitè Européen de Normalisation, Brussels.

42 Jeon JS, Park JH and DesRoches R (2015). "Seismic fragility of lightly reinforced concrete frames with masonry infills". *Earthquake Engineering and Structural Dynamics,* **44**(11): 1783-1803. https://doi.org/10.1002/eqe.2555

43 Rossetto T and Elnashai A (2003). "Derivation of vulnerability functions for European-type RC structures based on observational data". *Engineering Structures,* **25**(10): 1241-1263. https://doi.org/10.1016/S0141-0296(03)00060-9

44 Dhakal RP, Pourali A, Tasligedik AS, Yeow T, Baird A, MacRae G, Pampanin S and Palermo A (2016). "Seismic performance of non-structural components and contents in buildings: An overview of NZ research". *Earthquake Engineering and Engineering Vibration,* **15**: 1-17. https://doi.org/10.1007/s11803-016-0301-9

45 Bianchi S and Pampanin S (2022). "Fragility functions for architectural nonstructural components". *Journal of Structural Engineering,* **148**(10): 03122005. https://doi.org/10.1061/(ASCE)ST.1943-541X.000335

46 Thamboo J and Dhanasekar M (2019). "Correlation between the performance of solid masonry prisms and wallettes under compression". *Journal of Building Engineering,* **22**: 429–438. https://doi.org/10.1016/j.jobe.2019.01.007

47 Asteris PG, Lourenço PB, Hajihassani M, Adami CEN, Lemonis ME, Skentou AD, Marques R, Nguyen H, Rodrigues H and Varum H (2021). "Soft computing-based models for the prediction of masonry compressive strength". *Engineering Structures,* **248**: 113276. https://doi.org/10.1016/j.engstruct.2021.113276

48 CEN (2010). "*Eurocode 2. EN 1992-1-1 (2010): Design of Concrete Structures - Part 1-1: General Rules and Rules for Buildings*". Comitè Européen de Normalisation, Brussels.

49 Guljaš I, Penava D, Laughery L and Pujol S (2018). "Dynamic tests of a large-scale three-story RC structure with masonry infill walls". *Journal of Earthquake Engineering,* **24**: 1675–1703. https://doi.org/10.1080/13632469.2018.1475313

50 CEN (2010). "*Eurocode 6. EN 1996-1-1 (2002): Design of Masonry Structures - Part 1-1: Common Rules for Reinforced and Unreinforced Masonry Structures*". Comitè Européen de Normalisation, Brussels.

51 Mucedero G, Perrone D and Monteiro R (2022). "Epistemic uncertainty in poorly detailed existing frames accounting for masonry infill variability and RC shear failure". *Earthquake Engineering and Structural Dynamics,* **51**(15): 3755–3778. https://doi.org/10.1002/eqe.3748

52 De Risi MT, Di Domenico M, Manfredi V, Terrenzi M, Camata G, Mollaioli F and Verderame GM (2022). "Modelling and seismic response analysis of Italian pre-code and low-code reinforced concrete buildings. Part I: bare frames". *Journal of Earthquake Engineering,* **27**(6): 1482–1513. https://doi.org/10.1080/13632469.2022.2074919

53 Leuchars JM and Scrivener JC (1976). "Masonry infill panels subjected to cyclic in-plane loading". *Bulletin of the New Zealand Society for Earthquake Engineering,* **9**(2): 122-131. https://doi.org/10.5459/bnzsee.9.2.122-131

54 Zarnic R and Tomazevic M (1985). 'Study of the behaviour of masonry infilled reinforced concrete frames subjected to seismic loading". *7th International Conference on Brick Masonry*. Melbourne: Brick Development Research Institute.

55 Kato H, Goto T, Mizuno H and Liba M (1992). "Cyclic loading tests of confined masonry wall elements for structural design development of apartment houses in the third world". *10th World Conference on Earthquake Engineering*, Madrid, Vol. 10.

56 Angel R, Abrams DP, Shapiro D, Uzarski J and Webster M (1994). "*Behavior of reinforced concrete frames with masonry infills*" in *Civil Engineering Studies, SRS-589.* University of Illinois Engineering Experiment Station, College of Engineering, University of Illinois at Urbana-Champaign, IL, USA.

57 Haider S (1995). "*In-plane cyclic response of reinforced concrete frames with unreinforced masonry infills*". Rice University, USA.

58 Mehrabi AB, Shing PB, Schuller MP and Noland JL (1996). "Experimental evaluation of masonry-infilled RC frames". *Journal of Structural Engineering,* **122**(3): 228–237. https://doi.org/10.1061/(ASCE)0733-9445(1996)122:3(228)

59 Combescure D, Pires F, Cerqueira P and Pegon P (1996). "Test on masonry Infilled RC frames and its numerical interpretation". *Proceedings of the 11th World Conference on Earthquake Engineering*, UK: Pergamon.

60 Crisafulli FJ (1997). "*Seismic Behaviour of Reinforced Concrete Structures with Masonry Infills*". PhD Dissertation, Department of Civil Engineering, University of Canterbury, NZ.

61 Calvi GM and Bolognini D (2008). "Seismic response of reinforced concrete frames infilled with weakly reinforced masonry panels". *Journal of Earthquake Engineering*, **5**(2): 153–185.

62 Lafuente M, Molina A and Genatios C (2000). "Seismic resistant behavior of minor reinforced concrete frames with masonry infill walls". *12th World Conference on Earthquake Engineering,* Auckland, NZ.

63 Choi H, Nakano Y and Sanada Y (2005). "Seismic Performance and Crack Pattern of Concrete Block Infilled Frames." *Bulletin of Earthquake Resistant Structure Research Center* **38**: 119-134

64 Huang CH, Sung YC and Tsai CH (2006). "Experimental study and modeling of masonry infilled concrete frames with and without CFRP jacketing". *Structural Engineering and Mechanics*, **224**: 449–467. https://doi.org/10.12989/sem.2006.22.4.449

65 Bergami AV (2007). "*Implementation and experimental verification of models for nonlinear analysis of masonry infilled RC frames*". PhD Dissertation, Roma Tre University, Rome, Italy.

66 Altin S, Anil O, Kara ME and Kaya M (2008). "An experimental study on strengthening of masonry infilled RC frames using diagonal CFRP strips". *Compos Part B: Engineering*, **39**: 680–693. https://doi.org/10.1016/j.compositesb.2007.06.001

67 Kakaletsis DJ and Karayannis CG (2008). "Influence of masonry strength and openings on infilled R/C frames under cycling loading". *Journal of Earthquake Engineering,* **12**(2): 197–221. https://doi.org/10.1080/13632460701299138

68 Xu Q, Chen X, Chen JF, Harries KA, Chen L and Wang Z (2019). "Seismic strengthening of masonry walls using bamboo components". *Advances in Structural Engineering,* **22**(14): 2982-2997. https://doi.org/10.1177/1369433219855902

69 Imran L and Aryanto A (2009). "Behavior of reinforced concrete frames in-filled with lightweight materials under seismic loads". *Civil Engineering Dimension,* **11**(2): 69–77. https://doi.org/10.9744/ced.11.2.pp.%2069-77

70 Stavridis A (2009). "*Analytical and experimental study of seismic performance of reinforced concrete frames infilled with masonry walls*". PhD Dissertation, University of California, San Diego.

71 Tizapa SS (2009). "*Experimental and numerical study of confined masonry walls under in-plane loads. Case: Guerrero State (Mexico)".* PhD Dissertation, École Doctorale Materiaux-Ouvrages-Durabilité-Environnement-Structures, Université Paris-Est.

72 Waly AA (2010). "*Experimental and analytical work on the seismic performance of different types of masonry infilled reinforced concrete frames under cyclic loading*". Master's Thesis, Graduate School of Natural and Applied Sciences, Dokuz Eylül University.

73 Baran M and Sevil T (2010). "Analytical and experimental studies on infilled RC frames". *International Journal of the Physical Sciences*, **5**(13): 1981-1998.

74 Yuksel E and Teymur P (2011). "Earthquake performance improvement of low-rise RC buildings using high strength clay brick walls". *Bulletin of Earthquake Engineering,* **9**(4): 1157–1181. https://doi.org/10.1007/s10518-010-9242-2

75 Mansouri A, Marefat MS and Khanmohammadi M (2014). "Experimental evaluation of seismic performance of low-shear strength masonry infills with openings in reinforced concrete frames with deficient seismic details". *Structural Design of Tall and Special Buildings,* **23**(15): 1190–1210. https://doi.org/10.1002/tal.1115

76 Morandi P, Hak S and Magenes G (2014). "In-plane experimental response of strong masonry infills". *9th International Masonry Conference*, International Masonry Society, Whyteleafe, UK.

77 Bose S and Rai DC (2014). "Behavior of AAC infilled RC frame under lateral loading". *10th US National Conference on Earthquake Engineering*, Earthquake Engineering Research Institute, Oakland, CA.

78 Sigmund V and Penava D (2013). "Influence of openings, with and without confinement, on cyclic response of infilled R-C frames: An experimental study". *Journal of Earthquake Engineering,* **18**(1): 113–146. https://doi.org/10.1080/13632469.2013.817362

79 Bergami A and Nuti C (2015). "Experimental tests and global modeling of masonry infilled frames". *Earthquakes and Structures,* **9**(2): 281–303.

80 Schwarz S, Hanaor A and Yankelevsky DZ (2015). "Experimental response of reinforced concrete frames with AAC masonry infill walls to in-plane cyclic loading". *Structures,* **3**: 306–319. https://doi.org/10.1016/j.istruc.2015.06.005

81 Misir IS, Ozcelik O, Girgin SC and Yucel U (2016). "The behavior of infill walls in RC frames under combined bidirectional loading". *Journal of Earthquake Engineering,* **20**(4): 559–586. https://doi.org/10.1080/13632469.2015.1104748

82 Jiang H, Liu X and Mao J (2015). "Full-scale experimental study on masonry infilled RC moment-resisting frames under cyclic loads". *Engineering Structures*, **61**: 70–84. https://doi.org/10.1016/j.engstruct.2015.02.008

83 Dehghani A, Nateghi-Alahi F and Gregor F (2015). "Engineered cementitious composites for strengthening masonry infilled reinforced concrete frames". *Engineering Structures,* **105**: 197–208. https://doi.org/10.1016/j.engstruct.2015.10.013

84 Gazic G and Sigmund V (2016). "Cyclic testing of single-span weak frames with masonry infill". *Gradevinar,* **68**(8): 617–633.

85 Basha SH and Kaushik HB (2016). "Behavior and failure mechanisms of masonry-infilled RC frames (in low-rise buildings) subject to lateral loading". *Engineering Structures,* **111**: 233–245. https://doi.org/10.1016/j.engstruct.2015.12.034

86 Huang Q, Guo Z and Kuang JS (2016). "Designing infilled reinforced concrete frames with the 'strong frame-weak infill' principle". *Engineering Structures,* **123**: 341–53. https://doi.org/10.1016/j.engstruct.2016.05.024

87 Alwashali H, Torihata Y, Jin K and Maeda M (2018). "Experimental observations on the in-plane behaviour of masonry wall infilled RC frames; focusing on deformation limits and backbone curve". *Bulletin of Earthquake Engineering,* **16**(3): 1373-97. https://doi.org/10.1007/s10518-017-0248-x

88 Cai G and Su Q (2019). "Effect of infills on seismic performance of reinforced concrete frame structures—A full-scale experimental study." *Journal of Earthquake Engineering,* **23**: 1531–59. https://doi.org/10.1080/13632469.2017.1387194

89 Morandi P, Milanesi R and Magenes G (2018). "Innovative solution for seismic-resistant masonry infills with sliding joints: in-plane experimental performance". *Engineering Structures,* **2018**(176): 719–33. https://doi.org/10.1016/j.engstruct.2018.09.018

90 Dautaj AD, Kadiri Q and Kabashi N (2018). "Experimental study on the contribution of masonry infill in the behavior of RC frame under seismic loading". *Engineering Structures,* **165**: 27–37. https://doi.org/10.1016/j.engstruct.2018.03.013

91 Ismail N, El-Maaddawy T and Khattak N. "Quasi-static in-plane testing of FRCM strengthened non-ductile reinforced concrete frames with masonry infills". *Construction and Building Materials,* **186**: 1286-1298. https://doi.org/10.1016/j.conbuildmat.2018.07.230

92 Akhoundi F, Vasconcelos G, Lourenço PB, Silva LM, Cunha F and Fangueiro R (2018). "In-plane behavior of cavity masonry infills and strengthening with textile reinforced mortar". *Engineering Structures,* **156**: 145–160. https://doi.org/10.1016/j.engstruct.2017.11.002

93 Sen D, Torihata Y, Alwashali H, Islam S, Tafheem Z and Maeda M (2019). "Investigation of the ferro-cement laminated infilled masonry wall under cyclic lateral load". *Pacific Conference on Earthquake Engineering and Annual NZSEE Conference,* April 4-6, Auckland, NZ.

94 Binici B, Canbay E, Aldemir A, Demirel IO, Uzgan U, Eryurtlu Z, Bulbul K and Yakut A (2019). "Seismic behavior and improvement of autoclaved aerated concrete infill walls". *Engineering Structures,* **193**: 68–81. https://doi.org/10.1016/j.engstruct.2019.05.032

95 Han SW and Lee CS (2020). "Cyclic behavior of lightly reinforced concrete moment frames with partial- and full-height masonry walls". *Earthquake Spectra,* **36**(2): 599–628. https://doi.org/10.1177/8755293019899960

96 Deng M, Zhang W and Yang S (2020). "In-plane seismic behavior of autoclaved aerated concrete block masonry walls retrofitted with high ductile fiber-reinforced concrete". *Engineering Structures,* **219**: 110854. https://doi.org/10.1016/j.engstruct.2020.110854

97 Sakr MA, El-Khoriby SR, Seleemah AA, Aboelnour MM and Osama B (2021). "Experimental and numerical investigation on cyclic behavior of masonry infilled RC frames retrofitted with partially bonded CFRP strips". *Structures,* **33**: 2238–2252. https://doi.org/10.1016/j.istruc.2021.05.087

98 Lu X and Zha S (2021). "Full-scale experimental investigation of the in-plane seismic performance of a novel resilient infill wall". *Engineering Structures,* **232**: 111826. https://doi.org/10.1016/j.engstruct.2020.111826

99 Xie X, Zhang L and Qu Z (2020). "A critical review of methods for determining the damage states for the in-plane fragility of masonry infill walls". *Journal of Earthquake Engineering,* **26**(9): 4523-4544. https://doi.org/10.1080/13632469.2020.1835749

100 Aydin BB, Binici B, Hendriks MAN and Tuncay K (2022). "Lattice modeling and testing of aerated autoclaved concrete infilled frames". *Engineering Structures*, **251**: 113467. https://doi.org/10.1016/j.engstruct.2021.113467

101 Demirel IO, Binici B and Yakut A (2023). "In-plane seismic performance of different infill wall systems in ductile reinforced concrete frames". *Bulletin of Earthquake Engineering,* **21**: 3433–3459. https://doi.org/10.1007/s10518-023-01663-5

102 Rohatgi A (2014). *WebPlotDigitizer User Manual Version 3.4*. Available from: //efaidnbmnnnibpcajpcglclefindmkaj/https://automeris.io/WebPlotDigitizer/userManual.pdf

103 Kumar M, Rai DC and Jain SK (2015). "Ductility reduction factors for masonry-infilled reinforced concrete frames". *Earthquake Spectra,* **31**: 339–365. https://doi.org/10.1193/110512EQS322M

104 Trapani F D, Sberna AP and Marano GC (2021). "A new genetic algorithm-based framework for optimized design of steel-jacketing retrofitting in shear-critical and ductility-critical RC frame structures". *Engineering Structures,* **243**: 112684. https://doi.org/10.1016/j.engstruct.2021.112684

105 Bentz EC (2000). "*Sectional Analysis of Reinforced Concrete Members- Appendix A: Program Manuals*". PhD Dissertation, 2000:87, University of Toronto, Canada.

106 Bentz EC, Vecchio FJ and Collins MP (2006). "Simplified modified compression field theory for calculating shear strength of reinforced concrete elements". *ACI Structural Journal,* **103**: 614–24.

107 Elwood KJ (2004). "Modelling failures in existing reinforced concrete columns". *Canadian Journal of Civil Engineering*, **31**(5): 846–859. https://doi.org/10.1139/l04-040

108 Rajapakse R, Wijesundara K, Nascimbene R, Bandara C and Dissanayake R(2019). "Accounting axial-moment-shear interaction for force-based fiber modeling of RC frames". *Engineering Structures,* **184**: 15–36. https://doi.org/10.1016/j.engstruct.2019.01.075

109 Sathurshan M, Thamboo J, Mallikarachchi C and Wijesundara K (2023). "Seismic fragility of lightly reinforced concrete school building typologies with different masonry infill configureurations". *Structures*, **47**: 1710–1728. https://doi.org/10.1016/j.istruc.2022.12.014

110 Srechai J, Leelataviwat S, Wararuksajja W and Limkatanyu S (2022). "Multi-strut and empirical formula-based macro modeling for masonry infilled RC frames". *Engineering Structures,* **266**: 114559. https://doi.org/10.1016/j.engstruct.2022.114559

111 Burton H and Deierlein G (2014). "Simulation of seismic collapse in nonductile reinforced concrete frame buildings with masonry infills." *Journal of Structural Engineering,* **140**: A4014016. https://doi.org/10.1061/(ASCE)ST.1943-541X.0000921

112 Muguruma H, Nishiyama M, Watanabe F and Tanaka H (1991). "Ductile behavior of high-strength concrete columns confined by high strength transverse reinforcement". *Proceedings of the ACI International Conference*, **2**: 877– 891.

113 Del Zoppo M, Wijesundara K, Rossetto T, Dias P, Baiguera M, Di Ludovico M, Thamboo J and Prota A (2021). "Influence of exterior infill walls on the performance of RC frames under tsunami loads: Case study of school buildings in Sri Lanka". *Engineering Structures,* **234**: 111920. https://doi.org/10.1016/j.engstruct.2021.11192

114 FEMA P-58 (2012). "*Seismic Performance Assessment of Buildings: Vol. 1 – Methodology*". FEMA P-58-1, Prepared by the Applied Technology Council for the Federal Emergency Management Agency, Washington, D.C

SUPPLEMENTARY DATA A - MI-RC EXPERIMENTAL DATABASE USED

Reference	Specimen	MI dimension (mm)			Column size (mm)		Beam size (mm)		Column reinforcement (%)	Beam reinforcement (%)	Column transverse reinforcement (%)	Beam transverse reinforcement (%)	Column axial load (kN)	ND/D	f_m (MPa)	f_c (MPa)	Damage states drift ratios (%)			
		h	*l*	*t*	h_c	b_c	h_b	b_b									DS1	DS2	DS3	DS4
Leuchar & Scrivener (1976)	Unit2	1803	1168	120	203	152	203	152	4	2	0.01	0.01	0	ND	26.4	24.82	0.12	0.29	0.45	1.50
Zarnic & Tomazevic (1988)	S3	1080	680	-	-	-	-	-	-	-	-	-	-	ND	-	-	0.10	0.40	0.93	1.80
	S0	1080	680	-	-	-	-	-	-	-	-	-	-	ND	-	-	0.15	0.80	1.48	2.50
Kao et al (1992)	A	870	1330	100	200	100	450	-	4	-	1	-	-	ND	40.3	20.3	0.04	0.52	0.20	1.50
	B	870	1330	100	200	100	450	-	4	-	0.3	-	-	ND	40.3	20.3	0.10	0.20	0.21	0.78
	C	870	1330	100	200	100	450	-	0.9	-	1	-	-	ND	40.3	20.3	0.03	0.20	0.26	2.00
	D	870	1330	100	200	100	450	-	0.9	-	0.3	-	-	ND	40.3	20.3	0.02	0.10	0.13	0.50
Angel (1994)	2A	2438	1638	48	305	305	305	254	3.34	0.55	0.74	0.88	222	ND	11.0	56	0.08	0.28	0.30	0.30
	3A	2438	1638	48	305	305	305	254	3.34	0.55	0.74	0.88	222	ND	10.3	56	0.06	0.15	0.18	0.20
	4A	2438	1638	92	305	305	305	254	3.34	0.55	0.74	0.88	222	ND	23.3	56	0.20	0.50	0.63	0.67
	5A	2438	1638	143	305	305	305	254	3.34	0.55	0.74	0.88	222	ND	21.8	56	0.04	0.20	0.54	0.58
	6A	2438	1638	98	305	305	305	254	3.34	0.55	0.74	0.88	222	ND	4.7	56	0.09	0.19	0.22	0.23
	7A	2438	1638	98	305	305	305	254	3.34	0.55	0.74	0.88	222	ND	11.2	56	0.06	0.17	0.22	0.23
	8A	2438	1638	187	305	305	305	254	3.34	0.55	0.74	0.88	222	ND	2.7	56	0.10	0.30	0.34	0.40
Haidar (1995)	A	2210	2070	89	305	305	254	254	1.76	1.03	0.37	0.44	116.33	ND	10.8	36.3	0.30	0.80	0.97	2.00
	B	2210	2070	89	305	305	254	254	1.83	1.03	0.37	0.44	155.84	ND	12.1	36.3	0.48	1.10	1.47	3.47
	C	2210	2070	89	305	305	254	254	1.76	1.03	0.37	0.44	118.55	ND	18.1	36.3	0.40	1.10	1.48	1.50
	D	2210	2070	89	305	305	254	254	1.83	0.86	0.37	0.44	158.952	ND	16.7	36.3	0.41	0.80	1.00	1.11
Meharabi et al (1996)	Specimen-2	2032	1422	92	178	178	229	152.4	3	1.14	0.6	0.5	293.7	ND	9.7	30.86	0.01	0.03	0.09	0.12
	Specimen-11	2946	1422	92	178	178	229	152.4	3	1.14	0.6	0.5	195.8	ND	11.4	25.7	0.01	0.02	0.03	0.07
	Specimen-12	2946	1422	92	178	178	229	152.4	3	1.14	0.6	0.5	195.8	ND	13.6	26.8	0.00	0.01	0.02	0.04
	Specimen-3	2032	1422	92	178	178	229	152.4	3	1.14	0.6	0.5	293.7	ND	15.1	30.86	0.00	0.01	0.04	0.05
	Specimen-4	2032	1422	92	178	178	229	152.4	3	1.14	0.6	0.5	195.8	ND	10.6	30.86	0.00	0.01	0.02	0.06
	Specimen-5	2032	1422	92	178	178	229	152.4	3	1.14	0.8	1	195.8	ND	13.9	26.802	0.01	0.02	0.03	0.06
	Specimen-6	2032	1422	92	203	203	229	152.4	4	1.14	0.8	1	195.8	ND	10.1	20.877	0.00	0.01	0.02	0.06
	Specimen-7	2032	1422	92	203	203	229	152.4	4	1.14	0.6	0.5	195.8	ND	13.6	25.84	0.01	0.02	0.03	0.04
	Specimen-8	2032	1422	92	178	178	229	152.4	3	1.14	0.6	0.5	195.8	ND	9.5	33.42	0.00	0.02	0.04	0.08
	Specimen-9	2032	1422	92	178	178	229	152.4	-	1.14	0.6	0.5	195.8	ND	14.2	26.8	0.00	0.01	0.02	0.08
	Specimen-10	2946	1422	92	178	178	229	152.4	3	1.14	0.6	0.5	195.8	ND	10.6	26.8	-	-	-	-
Combescure et al (1996)	MD3	2250	1700	150	150	150	200	150	3	-	-	0	100	ND	-	-	0.20	0.40	0.60	0.66
	MD4	2250	1700	150	150	150	200	150	3	-	-	0	20	ND	-	-	0.19	0.25	0.91	1.10

Crisafulli (1997)	Unit1	2666	2100	75	150	150	200	150	1.4	0.5	1.1	0.38	20	ND	9.2	22.5	0.01	0.10	0.59	1.50
	Unit2	2666	2100	75	150	150	200	150	1.4	0.5	1.1	0.38	20	ND	9.2	31.2	0.01	0.10	0.88	2.00
Calvi & Bolognini (2001)	2	4200	3000	135	300	300	250	700	3	0.8	1	0.02	-	ND	1.1	29.32	0.02	0.20	0.41	1.20
	3	4200	3000	135	300	300	250	700	3	0.8	1	0.02	-	ND	1.1	29.32	0.18	0.10	2.17	4.00
	4	4200	3000	135	300	300	250	700	3	0.8	1	0.02	-	ND	1.1	29.32	0.09	0.20	2.15	4.00
	5	4200	3000	135	300	300	250	700	3	0.8	1	0.02	-	ND	1.1	29.32	0.02	0.10	0.24	3.50
	6	4200	3000	135	300	300	250	700	3	0.8	1	0.02	-	ND	1.1	29.32	0.08	0.17	0.19	0.31
	7	4200	3000	135	300	300	250	700	3	0.8	1	0.02	-	ND	1.1	29.32	0.05	0.23	0.27	0.44
	8	4200	3000	135	300	300	250	700	3	0.8	1	0.02	-	ND	1.1	29.32	0.07	0.09	0.21	0.40
	9	4200	3000	135	300	300	250	700	3	0.8	1	0.02	-	ND	1.1	29.32	0.06	0.12	0.25	0.44
Lafuente et al (2000)	1	1180	1944	120	120	120	200	120	3	1	2	2	0	ND	9.3	18	0.01	0.10	0.60	0.90
	2	1180	1944	120	120	120	200	120	3	1	2	2	0.93	ND	9.3	18	0.01	0.10	0.34	0.50
	3	1180	1944	120	120	120	200	120	3	1	2	2	0.46	ND	9.3	18	0.01	0.10	0.47	0.90
	4	1180	1211	120	120	120	200	120	3	1	2	2	0.7	ND	9.3	18	0.02	0.30	0.34	0.68
	5	1180	1211	120	120	120	200	120	3	1	2	2	0	ND	9.3	18	0.01	0.10	0.86	1.10
	6	1180	1211	120	120	120	200	120	3	1	2	2	0.93	ND	9.3	18	0.02	0.20	0.26	0.50
	7	1180	1468	120	120	120	200	120	3	1	2	2	1.39	ND	9.3	18	0.02	0.20	0.50	0.90
	8	1180	1468	120	120	120	200	120	3	1	2	2	0	ND	9.3	18	0.01	0.10	0.21	0.30
	9	1180	1468	120	120	120	200	120	3	1	2	2	0.46	ND	9.3	18	0.03	0.30	0.76	1.00
	10	1180	1468	120	120	120	200	120	3	1	2	2	0	ND	9.3	18	0.05	0.50	1.02	1.60
Choi et al (2005)	IW1	3600	2400	190	450	400	600	800	3	0.55	0.1	0.3	720	ND	10.3	27.3	0.10	0.40	0.67	1.50
	IW2	3600	2400	190	450	400	600	800	3	0.55	0.1	0.3	720	ND	10.3	29.6	0.10	0.40	0.67	2.00
Huang & Sung (2006)	BMNF10B	2500	1700	220	500	300	500	300	2	0.77	0.2	0.2	0	ND	6.4	19.7	0.20	0.80	1.27	2.00
Bergami (2007)	Ft1	2300	1300	120	200	200	250	200	0.5	0.47	0.2	0.2	159	ND	2.7	25.86	0.16	0.70	1.34	2.50
	Ft2	2300	1300	120	200	200	250	200	0.5	0.47	0.2	0.2	159	ND	2.7	25.86	0.10	0.30	0.37	1.50
Altin et al (2008)	1	1300	750	80	100	150	150	150	1	0.67	0.3	0.2	26	ND	2.8	17.3	0.01	0.20	0.26	0.80
Kakaletsis & Karyannis (2008)	S	1200	800	52	150	150	200	100	0.7	0.35	0.3	0.4	50	ND	2.6	22.81	0.14	0.90	1.20	2.80
	IS	1200	800	60	150	150	200	100	0.7	0.35	0.3	0.4	50	ND	15.2	22.81	0.13	0.90	1.37	3.80
Xu et al (2009)	W1	2112	1750	240	-	-	240	240	-	-	-	0	5kN on beam	ND	5.7		0.18	0.30	0.53	0.60
	W2	2115	1750	240	240	120	240	240	0.7	-	0.3	0	5kN on beam	ND	5.7	24.72	0.16	0.50	0.60	0.80
Imran & Aryanto (2009)	Model-1	1500	1500	117	175	175	250	150	2	1	0.5	0.6	0	ND	3.0	21.67	0.08	0.26	0.44	2.88
	Model-2	1500	1500	117	175	175	250	150	2	1	0.5	0.6	0	ND	3.7	20.86	0.08	0.41	0.62	3.00
Starvdis (2009)	CU1	3378	1864	100	279	279	368	279	1	0.5	0.01	0.01	0	ND	24.3	30	0.06	0.10	0.22	0.50
Tizapa (2009)	MMR3	2100	1800	125	250	125	200	125	1	0.5	0.5	0.5	0	ND	4.5	14	0.06	0.40	0.60	0.65
	MMR2	2100	1800	125	250	125	200	125	1	0.5	0.5	0.5	0	ND	4.5	24	0.20	0.30	0.44	0.69
	MUR2	2100	1800	125	250	125	200	125	1	0.5	0.5	0.5	0	ND	4.5	24	0.03	0.20	0.48	0.98

Waly (2010)	2	1750	1250	60	250	150	250	150	0.8	0.25	-	0	98.06	ND	2.2	18	0.14	0.30	0.67	2.44
	3	1750	120	75	250	150	250	150	0.8	0.2	-	0	98.06	ND	2.2	18	0.22	1.60	3.29	3.30
Baran & Sevil (2010)	SP7	1300	750	150	100	150	150	150	1	0.5	0.3	0.2	-	ND	-	15.6	0.02	0.30	0.33	1.30
	SP8	1300	750	150	100	150	150	150	1	0.5	0.3	0.2	-	ND	-	10.7	0.13	0.50	0.62	1.70
	SP9	1300	750	150	100	150	150	150	1	0.5	0.3	0.2	-	ND	-	9.7	0.03	0.40	0.59	1.90
Yuksel & Teymur (2011)	S0	1700	1170	102	250	200	325	200	2	0.55	0.2	0.1	0	ND	25.2	18	0.09	0.40	0.72	1.00
	S1	1700	1170	102	250	200	325	200	2	0.55	0.2	0.1	0	ND	25.2	18	0.10	0.40	0.74	1.00
Mansouri (2013)	S	2100	1300	106	200	200	150	200	2	0.5	0.4	0.6	78	ND	2.3	21.9	0.05	0.75	1.00	3.50
Morandi & Magenes (2014)	TA1	4220	2950	240	350	350	-	-	-	-	-	0	400	D	1.9	22.4	0.10	0.90	1.48	1.50
	TA2	4220	2950	240	350	350	-	-	-	-	-	0	400	D	1.9	22.4	0.10	0.25	1.00	2.50
	TA3	4220	2950	240	350	350	-	-	-	-	-	0	400	D	1.9	22.4	0.10	0.60	0.98	1.00
Bose & Rai (2014)	Infill	2200	1300	125	200	200	200	200	2	1.18	0.5	0.7	0	ND	2.4	20	0.02	0.10	0.18	0.40
	IF-AAC	2200	1300	125	200	200	200	200	2	1.18	0.5	0.7	0	ND	2.4	20	0.15	1.05	2.00	3.00
Sigmund & Penava (2014)	TypeIII-2	1800	1300	120	200	200	200	120	2	2	0.4	0.5	365	ND	5.2	25.2	0.06	0.20	0.26	1.10
Cavleri & Trapani (2014)	SIA-1	1600	1600	210	200	200	400	200	0.8	0.3	0.3	0.4	200	ND	2.7	20	0.10	0.30	0.64	1.60
	SIA-2	1600	1600	210	200	200	400	200	0.8	0.3	0.3	0.4	200	ND	2.7	20	0.10	0.50	1.08	2.50
	S2A-1	1600	1600	210	200	200	400	200	0.5	0.3	0.3	0.4	200	ND	3.9	20	0.10	0.20	0.59	0.60
	S2A-2	1600	1600	210	200	200	400	200	0.5	0.3	0.3	0.4	200	ND	3.9	20	0.10	0.30	0.64	0.70
	SIB-1	1600	1600	150	200	200	400	200	0.8	0.3	0.3	0.4	200	ND	4.2	20	0.02	0.30	0.69	1.50
	SIB-2	1600	1600	150	200	200	400	200	0.8	0.3	0.3	0.4	200	ND	4.2	20	0.01	0.10	0.46	1.10
	SIC-1	1600	1600	300	300	300	400	300	0.5	0.3	0.2	0.2	200	ND	0.3	20	0.01	0.50	1.11	1.80
	SIC-2	1600	1600	300	300	300	400	300	0.5	0.3	0.2	0.2	200	ND	0.3	20	0.01	0.50	1.06	1.70
	SIC-3	1600	1600	300	300	300	400	300	0.5	0.3	0.2	0.2	200	ND	0.3	20	0.01	0.30	0.94	2.30
	SIC-4	1600	1600	300	300	300	400	300	0.5	0.3	0.2	0.2	200	ND	0.3	20	0.01	0.50	0.71	1.80
Bergami & Nuti (2015)	Fn1	2300	1300	120	200	200	200	250	0.5	0.45	0.2	0.2	159	ND	2.2	-	-	-	-	-
	Ft1	2300	1300	120	200	200	200	250	0.5	0.45	0.2	0.2	159	ND	2.2	-	0.16	0.80	1.18	2.50
	Ft2	2300	1300	120	200	200	200	250	0.5	0.45	0.2	0.2	159	ND	2.2	-	0.05	0.30	0.37	1.20
Schwarz et al (2015)	1000	900	1400	100	100	200	200	200	0.8	0.64	0.07	0.07	125	ND	2.7	28.8	0.10	0.70	1.50	2.86
	1100	900	1400	100	100	200	200	200	0.8	0.64	0.07	0.07	125	ND	2.7	28.8	0.50	0.71	1.07	2.50
	0000	2045	1400	100	100	200	200	200	0.8	0.64	0.07	0.07	125	ND	2.7	28.8	0.71	1.10	1.40	2.86
	0100	2045	1400	100	100	200	200	200	0.8	0.64	0.07	0.07	125	ND	2.7	28.8	0.36	0.43	1.43	2.85
	0101	2045	1400	100	100	200	200	200	0.8	0.64	0.07	0.07	125	ND	2.7	28.8	0.36	0.44	1.42	2.85
Jiang et al (2015)	AFKJ1	5240	2725	200	400	400	450	250	2	1	0.4	0.4	600	D	3.5	22.8	0.13	0.15	0.68	1.47
	AFKJ2	5240	2725	200	400	400	450	250	2	1	0.4	0.4	600	D	3.5	22.8	0.27	0.15	0.72	1.88
	AFKJ3	5240	2725	200	400	400	450	250	2	1	0.4	0.4	600	D	3.5	22.8	0.17	0.16	0.71	1.84
	AFKJ4	5240	2725	200	400	400	450	250	2	1	0.4	0.4	600	D	3.5	22.8	0.18	0.15	0.75	1.77
	AFKJ5	5240	2725	200	400	400	450	250	2	1	0.4	0.4	600	D	3.5	22.8	0.18	0.16	0.70	1.68
	AFKJ6	5240	2725	200	400	400	450	250	2	1	0.4	0.4	600	D	3.5	22.8	0.14	0.16	0.71	2.71

Misir et al (2015)	SBF	2000	1250	150	250	150	250	150	1	0.25	1	1	75	D	6.5	20.1	0.07	0.50	1.40	2.72
	LBF	2000	1250	150	250	150	250	150	1	0.25	1	1	75	D	4.5	20.3	0.08	0.80	2.70	3.50
Dehghani et al (2015)	IF	2000	1350	100	200	200	250	200	2.3	0.7	0.2	0.3	-	ND	12.3	32.08	0.34	0.80	1.10	3.60
Gazic & Sigmund (2016)	1bpm	1850	1300	120	150	125	200	125	1	3.8	0.13	0.13	253	ND	6.7	16	0.09	0.20	0.27	0.85
	1bpm*	1850	1300	120	150	125	200	125	1	3.8	0.13	0.13	253	ND	6.7	16	0.08	0.20	0.27	0.88
	1cpm	1850	1300	120	150	125	200	125	1	3.8	0.13	0.13	253	ND	6.4	16	0.16	0.30	0.39	1.70
	1bvm	1850	1300	120	150	125	200	125	1	3.8	0.13	0.13	253	ND	6.7	16	0.06	0.10	0.16	1.00
	1cvm	1850	1300	120	150	125	200	125	1	3.8	0.13	0.13	253	ND	6.4	16	0.08	0.10	0.18	1.80
	2cpm	1850	1300	120	125	150	20	125	1	3.8	0.13	0.13	253	ND	6.4	16	0.16	0.30	0.41	0.99
	3bpm	1750	1300	120	250	125	200	125	1	3.8	0.13	0.13	253	ND	6.4	16	0.12	0.20	0.28	0.89
	3cpm	1750	1300	120	250	125	200	125	1	3.8	0.13	0.13	253	ND	6.4	16	0.15	0.30	0.50	1.35
	04bpm	1750	1300	120	250	125	250	125	1.29	3	0.13	0.13	253	ND	6.4	16	0.16	0.20	0.28	0.93
	04cpm	1750	1300	120	250	125	250	125	1.29	3	0.13	0.13	253	ND	6.4	16	0.24	0.43	0.70	1.62
Basha & Kaushik (2016)	DFS	1500	1500	110	175	115	175	115	2	0.75	0.5	0.8	0	ND	3.9	22.4	0.31	0.77	0.99	3.00
	DHS	1500	1500	55	175	115	175	115	2	0.75	0.5	0.8	0	ND	4.6	22.4	0.15	0.46	1.06	1.65
	NDFS	1500	1500	110	175	115	175	115	2	0.75	0.5	0.4	0	ND	3.9	22.4	0.31	0.46	1.40	3.00
	NDHS	1500	1500	55	175	115	175	115	2	0.75	0.5	0.4	0	ND	4.6	22.4	0.15	0.62	0.70	3.10
	DISC	1500	1500	110	175	115	175	115	2	0.75	0.5	0.4	0	ND	3.9	22.4	0.31	0.77	1.80	3.50
	DISCSB	1500	1500	110	175	115	175	115	2	0.75	0.5	0.4	0	ND	3.9	22.4	0.46	0.77	0.80	3.70
	DISTL	1500	1500	110	175	115	175	115	2	0.75	0.5	0.4	0	ND	3.9	22.4	0.31	0.92	1.40	3.60
Huang et al (2016)	IF-1	2000	1250	120	250	250	250	200	1	0.35	0.5	0.4	328	ND	5.4	34.5	0.11	0.33	0.57	4.05
	IF-2	2000	1250	180	250	250	250	200	1	0.35	0.5	0.4	328	ND	2.3	34.5	0.10	0.33	0.52	3.50
	IF-3	2000	1250	180	250	250	250	200	1	0.35	0.5	0.4	328	ND	2.3	34.5	0.10	0.31	0.57	1.54
	IF-4	2000	1250	120	250	250	250	200	1	0.35	0.5	0.4	328	ND	2.5	34.5	0.10	0.20	0.54	4.10
Alwashali et al (2017)	WF	2100	1400	100	200	200	400	600	0.8	0.75	0.3	0.4	200	ND	17.3	24.2	0.05	0.13	0.20	2.00
	SF	2100	1400	100	300	300	400	600	1.8	0.75	0.6	0.4	200	ND	18.6	28.3	0.06	0.33	0.60	2.00
Cai & Su (2017)	0%	3000	3500	200	400	400	600	500	0.8	0.2	0.3	0.2	572	D	2.0	33.5	0.05	0.50	0.75	1.50
Morandi et al (2018)	TA1	4220	2950	235	350	350	350	350	2	0.5	0.6	0.8	400	ND	4.6	34	0.10	0.50	1.50	2.50
Dautaj et al (2018)	1	-	-	-	150	150	200	150	2	1	0.5	0.5	20	ND	-	-	-	-	-	-
	2	2500	2000	120	150	150	200	150	2	1	0.5	0.5	20	ND	2.0	19.6	0.30	1.10	1.90	3.00
	6	2500	2000	120	200	150	200	150	2	1	0.5	0.5	20	ND	2.0	19.6	0.26	1.02	1.70	2.80
	8	2400	2000	120	200	150	200	150	2	1	0.5	0.5	20	ND	2.0	19.2	0.18	0.90	1.40	2.50
	9	2400	2000	120	200	150	200	150	2	1	0.5	0.5	20	ND	2.0	19.6	0.16	0.85	1.50	2.40
	10	2300	1950	120	250	150	250	150	1	0.5	0.5	0.5	20	ND	2.0	20	0.24	0.90	1.50	4.00
	11	2400	2000	120	150	150	200	150	2	1	0.5	0.5	20	ND	-	19.2	0.13	0.74	1.35	1.50
	13	2200	1900	120	300	150	300	150	1	0.5	0.5	0.5	20	ND	2.7	19.6	0.28	1.20	1.90	3.80

Ismail et al (2018)	IF-2	2270	1670	150	230	170	330	170	1.7	0.5	0.3	0.3	120	ND	5.3	25.7	0.30	1.00	1.75	2.00
Akhoundi et al (2018)	SIF-I-A	2703	2121	162	270	160	160	160	0.8	0.13	-	0	160	ND	1.2	20	0.10	0.40	0.47	2.25
	SIF-I(0.3%)-B	2703	2121	162	270	160	160	160	0.8	0.13	-	0	160	ND	1.2	20	0.10	0.20	0.27	0.28
	SIF-I(0.5%)-B	2703	2121	162	270	160	160	160	0.8	0.13	-	0	160	ND	1.2	20	0.10	0.20	0.28	0.46
	SIF-I(1%)-B	2703	2121	162	270	160	160	160	0.8	0.13	-	0	160	ND	1.2	20	0.30	0.78	0.90	1.00
Sent et al (2019)	IM	2100	1400	100	200	200	400	200	0.8	-	0.3	0	200	ND	17.3	24.2	0.05	0.20	0.80	2.00
Binici et al (2019)	S2	2300	1300	100	200	200	200	150	1	0.5	0.6	0.8	200	D	2.7	32.35	0.35	1.30	2.50	4.50
	S3	2300	1300	100	200	200	200	150	1	0.5	0.6	0.8	200	D	2.5	24.87	0.50	2.00	2.50	3.00
	S4	2300	1300	100	200	200	200	150	1	0.5	0.6	0.8	200	D	2.5	24.9	1.00	2.50	3.00	4.00
Han et al (2020)	S-Full	1470	1680	100	210	210	-	-	2	0.05		0	230	ND	8.4	25.6	0.57	0.80	1.10	1.70
Deng et al (2020)	CW-1	2400	1400	190	190	120	-	-	1	-	0.1	0	0	ND	1.8	11.92	-	-	-	-
	W1	2400	1400	190	-	-	-	-	-	-	-	0	0	ND	1.8	11.92	-	-	-	-
Sakr et al (2021)	IF	1200	1250	200	250	120	250	120	1	0.5	0.6	0.6	0	ND	-	33	0.50	0.70	1.13	1.26
Lu & Zha (2021)	OIW	3200	2430	200	400	400	400	250	1	0.94	0.38	0.4	800	D	2.6	-	0.10	0.20	2.00	2.86
Xie et al (2022)	H1	5000	3700	197	500	500	500	300	1.82	1.11	0.63	0.19	0	D	1.0	13.6	0.05	0.20	0.52	1.00
	H2	5000	3700	197	500	500	500	300	1.82	1.11	0.63	0.19	0	D	1.0	13.6	0.05	0.20	0.52	1.00
	H3	5000	3700	197	500	500	500	300	1.82	1.11	0.63	0.19	0	D	1.0	13.6	0.05	0.20	0.52	1.00
	S1	5000	3700	122	500	500	500	300	1.82	1.11	0.63	0.19	0	D	10.0	13.6	0.05	0.52	1.00	2.00
	S2	5000	3700	122	500	500	500	300	1.82	1.11	0.63	0.19	0	D	10.0	13.6	0.05	0.52	1.00	2.10
	S3	5000	3700	122	500	500	500	300	1.82	1.11	0.63	0.19	0	D	10.0	13.6	0.05	0.52	1.00	2.08
Aydin et al (2022)	SP1	2300	1400	100	200	200	200	150	1	0.75	0.85	0.75	180	D	1.0	25	0.35	0.50	1.00	3.00
Demiral (2023)	IF1	2300	1300	100	200	200	200	150	1	0.5	0.85	1.13	-	D	1.1	22.3	0.39	1.00	1.50	2.50

SUPPLEMENTARY DATA B - THE INPUT PARAMETERS USED FOR THE MI-RC FRAME VALIDATION

Material Model	Parameters	Akhoundi et al [79]	Jiang et al [69]
Concrete	xp	2	2
	xn	2.3	2.3
	r	2.91	3.58
Steel	b	0.0156	0.0025
	R0	12	12
	cR1	0.925	0.925
	cR2	0.15	0.15
Pinchin04	ePf1	0.05	0.20
	ePd1	0.0002	0.00025
	ePf2	0.225	1.152
	ePd2	0.002	0.0043
	ePf3	0.30	1.20
	ePd3	0.0032	0.012
	ePf4	0.28	1.05
	ePd4	0.0038	0.015
	eNf1	5	20
	eNd1	0.0002	0.00025
	eNf2	25	115.2
	eNd2	0.002	0.0043
	eNf3	30	120
	eNd3	0.0032	0.012
	eNf4	28	105
	eNd4	0.0038	0.015
	gK1	0	0
	gK2	0	0
	gK3	-11.46	-11.46
	gK4	0.16	0.15
	gKLim	0.22	0.21
	gD1	0.13	0.13
	gD2	0.69	0.9
	gD3	0	0
	gD4	0.22	0.26
	gDLim	0	0
	gF1	0.75	0.75
	gF2	0	0
	gF3	0.98	0.98
	gF4	0	0
	gFLim	0.18	0.18
	gE	10	0.1
	dmgType	cycle	cycle

SUPPLEMENTARY DATA C - MI-RC NUMERICALLY DEVELOPED DATABASE

Gap	Specimen	MI dimension (mm)			Column size (mm)		Beam size (mm)		Column reinforcement (%)	Beam reinforcement (%)	Column transverse reinforcement (%)	Beam transverse reinforcement (%)	Column axial load (kN)	ND/D	f_m (MPa)	f_c (MPa)	Damage states drift ratios (%)			
		h	*l*	*t*	h_c	b_c	h_b	b_b									DS1	DS2	DS3	DS4
Gap-01	2-25-0.67-1.31-D	3000	2000	200	350	350	300	250	1.31	1.6	0.57	0.15	306.25	D	2.0	25	0.17	0.67	1.72	4.44
	2-25-0.67-2.05-D	3000	2000	200	350	350	300	250	2.05	1.6	0.57	0.15	306.25	D	2.0	25	0.13	0.67	1.72	4.35
	2-25-0.5-1.31-D	3000	1500	200	350	350	300	250	1.31	1.6	0.57	0.15	306.25	D	2.0	25	0.20	0.67	1.72	4.63
	2-25-0.5-2.05-D	3000	1500	200	350	350	300	250	2.05	1.6	0.57	0.15	306.25	D	2.0	25	0.17	0.67	2.04	5.53
	2-35-0.67-1.31-D	3000	2000	200	350	350	300	250	1.31	1.6	0.57	0.15	367.5	D	2.0	35	0.17	0.67	1.92	3.37
	2-35-0.67-2.05-D	3000	2000	200	350	350	300	250	2.05	1.6	0.57	0.15	367.5	D	2.0	35	0.13	0.67	1.72	5.40
	2-35-0.5-1.31-D	3000	1500	200	350	350	300	250	1.31	1.6	0.57	0.15	367.5	D	2.0	35	0.20	0.67	1.72	5.01
	2-35-0.5-2.05-D	3000	1500	200	350	350	300	250	2.05	1.6	0.57	0.15	367.5	D	2.0	35	0.20	0.67	2.04	3.52
	4-25-0.67-1.31-D	3000	2000	200	350	350	300	250	1.31	1.6	0.57	0.15	306.25	D	4.0	25	0.10	0.33	1.72	4.76
	4-25-0.67-2.05-D	3000	2000	200	350	350	300	250	2.05	1.6	0.57	0.15	306.25	D	4.0	25	0.13	0.33	0.95	5.42
	4-25-0.5-1.31-D	3000	1500	200	350	350	300	250	1.31	1.6	0.57	0.15	306.25	D	4.0	25	0.17	0.67	1.61	4.88
	4-25-0.5-2.05-D	3000	1500	200	350	350	300	250	2.05	1.6	0.57	0.15	306.25	D	4.0	25	0.17	0.67	1.92	3.78
	4-35-0.67-1.31-D	3000	2000	200	350	350	300	250	1.31	1.6	0.57	0.15	367.5	D	4.0	35	0.13	0.33	1.41	5.00
	4-35-0.67-2.05-D	3000	2000	200	350	350	300	250	2.05	1.6	0.57	0.15	367.5	D	4.0	35	0.13	0.33	1.19	4.28
	4-35-0.5-1.31-D	3000	1500	200	350	350	300	250	1.31	1.6	0.57	0.15	367.5	D	4.0	35	0.13	0.67	1.89	4.89
	4-35-0.5-2.05-D	3000	1500	200	350	350	300	250	2.05	1.6	0.57	0.15	367.5	D	4.0	35	0.17	0.67	1.72	3.88
Gap-02	2-25-0.67-1.79-ND	3000	2000	200	300	300	300	250	1.79	1.6	0.22	0.15	225	ND	2.0	25	0.17	0.67	0.96	2.80
	2-25-0.67-2.79-ND	3000	2000	200	300	300	300	250	2.79	1.6	0.22	0.15	225	ND	2.0	25	0.17	0.67	1.00	2.12
	2-25-0.5-1.79-ND	3000	1500	200	300	300	300	250	1.79	1.6	0.22	0.15	225	ND	2.0	25	0.20	0.67	0.93	1.41
	2-25-0.5-2.79-ND	3000	1500	200	300	300	300	250	2.79	1.6	0.22	0.15	225	ND	2.0	25	0.20	0.67	0.96	1.21
	2-35-0.67-1.79-ND	3000	2000	200	300	300	300	250	1.79	1.6	0.22	0.15	270	ND	2.0	35	0.67	1.00	1.72	3.33
	2-35-0.67-1.79-ND	3000	2000	200	300	300	300	250	2.79	1.6	0.22	0.15	270	ND	2.0	35	0.13	0.47	2.12	3.33
	2-35-0.5-1.79-ND	3000	1500	200	300	300	300	250	1.79	1.6	0.22	0.15	270	ND	2.0	35	0.20	0.67	1.72	3.16
	2-35-0.5-2.79-ND	3000	1500	200	300	300	300	250	2.79	1.6	0.22	0.15	270	ND	2.0	35	0.17	0.67	0.95	2.49
	4-25-0.67-1.79-ND	3000	2000	200	300	300	300	250	1.79	1.6	0.22	0.15	225	ND	4.0	25	0.13	0.33	0.96	1.71
	4-25-0.67-2.79-ND	3000	2000	200	300	300	300	250	2.79	1.6	0.22	0.15	225	ND	4.0	25	0.13	0.33	0.95	1.20
	4-25-0.5-1.79-ND	3000	1500	200	300	300	300	250	1.79	1.6	0.22	0.15	225	ND	4.0	25	0.17	0.67	0.96	1.68
	4-25-0.5-2.79-ND	3000	1500	200	300	300	300	250	2.79	1.6	0.22	0.15	225	ND	4.0	25	0.17	0.67	0.95	1.22
	4-35-0.67-1.79-ND	3000	2000	200	300	300	300	250	1.79	1.6	0.22	0.15	270	ND	4.0	35	0.10	0.33	1.71	2.99
	4-35-0.67-2.79-ND	3000	2000	200	300	300	300	250	2.79	1.6	0.22	0.15	270	ND	4.0	35	0.13	0.43	0.95	2.36
	4-35-0.5-1.79-ND	3000	1500	200	300	300	300	250	1.79	1.6	0.22	0.15	270	ND	4.0	35	0.17	0.67	1.84	3.24
	4-35-0.5-2.79-ND	3000	1500	200	300	300	300	250	2.79	1.6	0.22	0.15	270	ND	4.0	35	0.13	0.67	0.95	2.99

Gap-03	7.5-25-1.33-0.50-ND	3000	4000	200	300	300	300	250	0.50	1.6	0.22	0.15	225	ND	7.5	25	0.10	0.33	0.34	2.49
	7.5-25-1.33-0.75-ND	3000	4000	200	300	300	300	250	0.75	1.6	0.22	0.15	225	ND	7.5	25	0.10	0.17	0.33	2.84
	7.5-25-1.00-0.50-ND	3000	3000	200	300	300	300	250	0.50	1.6	0.22	0.15	225	ND	7.5	25	0.11	0.33	0.57	0.62
	7.5-25-1.00-0.75-ND	3000	3000	200	300	300	300	250	0.75	1.6	0.22	0.15	225	ND	7.5	25	0.10	0.33	0.59	0.65
	7.5-35-1.33-0.50-ND	3000	4000	200	300	300	300	250	0.50	1.6	0.22	0.15	315	ND	7.5	35	0.10	0.47	0.36	0.55
	7.5-35-1.33-0.75-ND	3000	4000	200	300	300	300	250	0.75	1.6	0.22	0.15	315	ND	7.5	35	0.10	0.33	0.31	0.47
	7.5-35-1.00-0.50-ND	3000	3000	200	300	300	300	250	0.50	1.6	0.22	0.15	315	ND	7.5	35	0.10	0.33	0.59	0.62
	7.5-35-1.00-0.75-ND	3000	3000	200	300	300	300	250	0.75	1.6	0.22	0.15	315	ND	7.5	35	0.10	0.33	0.65	0.78
	10-25-1.33-0.50-ND	3000	4000	200	300	300	300	250	0.50	1.6	0.22	0.15	225	ND	10.0	25	0.10	0.33	0.35	0.48
	10-25-1.33-0.75-ND	3000	4000	200	300	300	300	250	0.75	1.6	0.22	0.15	225	ND	10.0	25	0.09	0.30	0.33	0.44
	10-25-1.00-0.50-ND	3000	3000	200	300	300	300	250	0.50	1.6	0.22	0.15	225	ND	10.0	25	0.10	0.40	0.33	0.40
	10-25-1.00-0.75-ND	3000	3000	200	300	300	300	250	0.75	1.6	0.22	0.15	225	ND	10.0	25	0.10	0.37	0.32	0.38
	10-35-1.33-0.50-ND	3000	4000	200	300	300	300	250	0.50	1.6	0.22	0.15	315	ND	10.0	35	0.10	0.50	0.33	0.49
	10-35-1.33-0.75-ND	3000	4000	200	300	300	300	250	0.75	1.6	0.22	0.15	315	ND	10.0	35	0.10	0.32	0.33	4.20
	10-35-1.00-0.50-ND	3000	3000	200	300	300	300	250	0.50	1.6	0.22	0.15	315	ND	10.0	35	0.10	0.50	0.33	0.50
	10-35-1.00-0.75-ND	3000	3000	200	300	300	300	250	0.75	1.6	0.22	0.15	315	ND	10.0	35	0.10	0.33	0.32	2.20
	12.5-25-1.33-0.50-ND	3000	4000	200	300	300	300	250	0.50	1.6	0.22	0.15	225	ND	12.5	25	0.09	0.40	0.31	0.32
	12.5-25-1.33-0.75-ND	3000	4000	200	300	300	300	250	0.75	1.6	0.22	0.15	225	ND	12.5	25	0.07	0.31	0.32	0.41
	12.5-25-1.00-0.50-ND	3000	3000	200	300	300	300	250	0.50	1.6	0.22	0.15	225	ND	12.5	25	0.10	0.47	0.31	3.89
	12.5-25-1.00-0.75-ND	3000	3000	200	300	300	300	250	0.75	1.6	0.22	0.15	225	ND	12.5	25	0.09	0.37	0.32	0.80
	12.5-35-1.33-0.50-ND	3000	4000	200	300	300	300	250	0.50	1.6	0.22	0.15	315	ND	12.5	35	0.09	0.37	0.31	0.45
	12.5-35-1.33-0.75-ND	3000	4000	200	300	300	300	250	0.75	1.6	0.22	0.15	315	ND	12.5	35	0.09	0.32	0.32	0.37
	12.5-35-1.00-0.50-ND	3000	3000	200	300	300	300	250	0.50	1.6	0.22	0.15	315	ND	12.5	35	0.09	0.37	0.32	0.37
	12.5-35-1.00-0.75-ND	3000	3000	200	300	300	300	250	0.75	1.6	0.22	0.15	315	ND	12.5	35	0.09	0.36	0.31	0.35
Gap-04	7.5-25-0.67-1.79-ND	3000	2000	200	300	300	300	250	1.79	1.6	0.22	0.15	225	ND	7.5	25	0.11	0.31	0.33	2.46
	7.5-25-0.67-2.79-ND	3000	2000	200	300	300	300	250	2.79	1.6	0.22	0.15	225	ND	7.5	25	0.11	0.15	0.32	2.81
	7.5-25-0.50-1.79-ND	3000	1500	200	300	300	300	250	1.79	1.6	0.22	0.15	225	ND	7.5	25	0.12	0.31	0.56	0.59
	7.5-25-0.50-2.79-ND	3000	1500	200	300	300	300	250	2.79	1.6	0.22	0.15	225	ND	7.5	25	0.11	0.31	0.58	0.62
	7.5-35-0.67-1.79-ND	3000	2000	200	300	300	300	250	1.79	1.6	0.22	0.15	315	ND	7.5	35	0.11	0.45	0.35	0.52
	7.5-35-0.67-2.79-ND	3000	2000	200	300	300	300	250	2.79	1.6	0.22	0.15	315	ND	7.5	35	0.11	0.31	0.30	0.44
	7.5-35-0.50-1.79-ND	3000	1500	200	300	300	300	250	1.79	1.6	0.22	0.15	315	ND	7.5	35	0.11	0.31	0.58	0.59
	7.5-35-0.50-2.79-ND	3000	1500	200	300	300	300	250	2.79	1.6	0.22	0.15	315	ND	7.5	35	0.11	0.32	0.64	0.75
	10-25-0.67-1.79-ND	3000	2000	200	300	300	300	250	1.79	1.6	0.22	0.15	225	ND	10.0	25	0.11	0.32	0.34	0.45
	10-25-0.67-2.79-ND	3000	2000	200	300	300	300	250	2.79	1.6	0.22	0.15	225	ND	10.0	25	0.10	0.29	0.32	0.43
	10-25-0.50-1.79-ND	3000	1500	200	300	300	300	250	1.79	1.6	0.22	0.15	225	ND	10.0	25	0.09	0.39	0.32	0.39
	10-25-0.50-2.79-ND	3000	1500	200	300	300	300	250	2.79	1.6	0.22	0.15	225	ND	10.0	25	0.09	0.36	0.30	0.37
	10-35-0.67-1.79-ND	3000	2000	200	300	300	300	250	1.79	1.6	0.22	0.15	315	ND	10.0	35	0.09	0.49	0.31	0.48

	10-35-0.67-2.79-ND	3000	2000	200	300	300	300	250	2.79	1.6	0.22	0.15	315	ND	10.0	35	0.09	0.31	0.31	4.19
	10-35-0.50-1.79-ND	3000	1500	200	300	300	300	250	1.79	1.6	0.22	0.15	315	ND	10.0	35	0.09	0.49	0.31	0.49
	10-35-0.50-2.79-ND	3000	1500	200	300	300	300	250	2.79	1.6	0.22	0.15	315	ND	10.0	35	0.09	0.32	0.30	2.19
	12.5-25-0.67-1.79-ND	3000	2000	200	300	300	300	250	1.79	1.6	0.22	0.15	225	ND	12.5	25	0.08	0.39	0.29	0.31
	12.5-25-0.67-2.79-ND	3000	2000	200	300	300	300	250	2.79	1.6	0.22	0.15	225	ND	12.5	25	0.06	0.30	0.30	0.40
	12.5-25-0.50-1.79-ND	3000	1500	200	300	300	300	250	1.79	1.6	0.22	0.15	225	ND	12.5	25	0.09	0.46	0.29	3.88
	12.5-25-0.50-2.79-ND	3000	1500	200	300	300	300	250	2.79	1.6	0.22	0.15	225	ND	12.5	25	0.08	0.36	0.30	0.79
	12.5-35-0.67-1.79-ND	3000	2000	200	300	300	300	250	1.79	1.6	0.22	0.15	315	ND	12.5	35	0.08	0.36	0.29	0.41
	12.5-35-0.67-2.79-ND	3000	2000	200	300	300	300	250	2.79	1.6	0.22	0.15	315	ND	12.5	35	0.08	0.31	0.30	0.33
	12.5-35-0.50-1.79-ND	3000	1500	200	300	300	300	250	1.79	1.6	0.22	0.15	315	ND	12.5	35	0.08	0.36	0.30	0.33
	12.5-35-0.50-2.79-ND	3000	1500	200	300	300	300	250	2.79	1.6	0.22	0.15	315	ND	12.5	35	0.08	0.35	0.29	0.31
Gap-05	7.5-25-0.67-1.31-D	3000	2000	200	350	350	300	250	1.31	1.6	0.57	0.15	306.25	D	7.5	25	0.11	0.37	1.87	4.10
	7.5-25-0.67-2.05-D	3000	2000	200	350	350	300	250	2.05	1.6	0.57	0.15	306.25	D	7.5	25	0.11	0.53	1.72	3.05
	7.5-25-0.50-1.31-D	3000	1500	200	350	350	300	250	1.31	1.6	0.57	0.15	306.25	D	7.5	25	0.13	0.53	1.71	2.73
	7.5-25-0.50-2.05-D	3000	1500	200	350	350	300	250	2.05	1.6	0.57	0.15	306.25	D	7.5	25	0.13	0.53	1.72	3.80
	7.5-35-0.67-1.31-D	3000	2000	200	350	350	300	250	1.31	1.6	0.57	0.15	428.75	D	7.5	35	0.11	0.34	1.92	3.26
	7.5-35-0.67-2.05-D	3000	2000	200	350	350	300	250	2.05	1.6	0.57	0.15	428.75	D	7.5	35	0.11	0.43	1.80	4.05
	7.5-35-0.50-1.31-D	3000	1500	200	350	350	300	250	1.31	1.6	0.57	0.15	428.75	D	7.5	35	0.13	0.47	1.53	3.61
	7.5-35-0.50-2.05-D	3000	1500	200	350	350	300	250	2.05	1.6	0.57	0.15	428.75	D	7.5	35	0.13	0.47	1.80	3.98
	10-25-0.67-1.31-D	3000	2000	200	350	350	300	250	1.31	1.6	0.57	0.15	306.25	D	10.0	25	0.11	0.38	1.58	3.56
	10-25-0.67-2.05-D	3000	2000	200	350	350	300	250	2.05	1.6	0.57	0.15	306.25	D	10.0	25	0.13	0.53	2.41	5.04
	10-25-0.50-1.31-D	3000	1500	200	350	350	300	250	1.31	1.6	0.57	0.15	306.25	D	10.0	25	0.13	0.53	1.72	2.84
	10-25-0.50-2.05-D	3000	1500	200	350	350	300	250	2.05	1.6	0.57	0.15	306.25	D	10.0	25	0.14	0.56	1.72	3.66
	10-35-0.67-1.31-D	3000	2000	200	350	350	300	250	1.31	1.6	0.57	0.15	428.75	D	10.0	35	0.11	0.37	1.60	3.80
	10-35-0.67-2.05-D	3000	2000	200	350	350	300	250	2.05	1.6	0.57	0.15	428.75	D	10.0	35	0.11	0.43	1.73	4.08
	10-35-0.50-1.31-D	3000	1500	200	350	350	300	250	1.31	1.6	0.57	0.15	428.75	D	10.0	35	0.13	0.50	1.56	3.69
	10-35-0.50-2.05-D	3000	1500	200	350	350	300	250	2.05	1.6	0.57	0.15	428.75	D	10.0	35	0.13	0.50	1.84	3.81
	12.5-25-0.67-1.31-D	3000	2000	200	350	350	300	250	1.31	1.6	0.57	0.15	306.25	D	12.5	25	0.11	0.55	1.71	3.28
	12.5-25-0.67-2.05-D	3000	2000	200	350	350	300	250	2.05	1.6	0.57	0.15	306.25	D	12.5	25	0.13	0.55	1.72	4.20
	12.5-25-0.50-1.31-D	3000	1500	200	350	350	300	250	1.31	1.6	0.57	0.15	306.25	D	12.5	25	0.17	0.65	2.39	4.44
	12.5-25-0.50-2.05-D	3000	1500	200	350	350	300	250	2.05	1.6	0.57	0.15	306.25	D	12.5	25	0.17	0.57	1.69	3.61
	12.5-35-0.67-1.31-D	3000	2000	200	350	350	300	250	1.31	1.6	0.57	0.15	428.75	D	12.5	35	0.10	0.53	1.43	3.48
	12.5-35-0.67-2.05-D	3000	2000	200	350	350	300	250	2.05	1.6	0.57	0.15	428.75	D	12.5	35	0.09	0.43	1.93	3.91
	12.5-35-0.50-1.31-D	3000	1500	200	350	350	300	250	1.31	1.6	0.57	0.15	428.75	D	12.5	35	0.17	0.53	1.65	3.50
	12.5-35-0.50-2.05-D	3000	1500	200	350	350	300	250	2.05	1.6	0.57	0.15	428.75	D	12.5	35	0.13	0.50	1.56	3.64

Gap-06	7.5-25-0.67-1.79-ND	3000	2000	200	300	300	300	250	1.79	1.6	0.57	0.15	225	ND	7.5	25	0.11	0.37	0.94	0.98
	7.5-25-0.67-2.79-ND	3000	2000	200	300	300	300	250	2.79	1.6	0.57	0.15	225	ND	7.5	25	0.11	0.38	0.80	1.00
	7.5-25-0.50-1.79-ND	3000	1500	200	300	300	300	250	1.79	1.6	0.57	0.15	225	ND	7.5	25	0.14	0.44	0.61	3.04
	7.5-25-0.50-2.79-ND	3000	1500	200	300	300	300	250	2.79	1.6	0.57	0.15	225	ND	7.5	25	0.13	0.51	1.65	2.88
	7.5-35-0.67-1.79-ND	3000	2000	200	300	300	300	250	1.79	1.6	0.57	0.15	315	ND	7.5	35	0.12	0.53	1.55	2.75
	7.5-35-0.67-2.79-ND	3000	2000	200	300	300	300	250	2.79	1.6	0.57	0.15	315	ND	7.5	35	0.12	0.38	1.53	2.99
	7.5-35-0.50-1.79-ND	3000	1500	200	300	300	300	250	1.79	1.6	0.57	0.15	315	ND	7.5	35	0.13	0.45	0.61	3.15
	7.5-35-0.50-2.79-ND	3000	1500	200	300	300	300	250	2.79	1.6	0.57	0.15	315	ND	7.5	35	0.15	0.45	1.83	2.58
	10-25-0.67-1.79-ND	3000	2000	200	300	300	300	250	1.79	1.6	0.57	0.15	225	ND	10.0	25	0.10	0.56	2.26	4.90
	10-25-0.67-2.79-ND	3000	2000	200	300	300	300	250	2.79	1.6	0.57	0.15	225	ND	10.0	25	0.10	0.42	2.29	2.17
	10-25-0.50-1.79-ND	3000	1500	200	300	300	300	250	1.79	1.6	0.57	0.15	225	ND	10.0	25	0.13	0.59	1.99	5.09
	10-25-0.50-2.79-ND	3000	1500	200	300	300	300	250	2.79	1.6	0.57	0.15	225	ND	10.0	25	0.13	0.59	1.72	2.99
	10-35-0.67-1.79-ND	3000	2000	200	300	300	300	250	1.79	1.6	0.57	0.15	315	ND	10.0	35	0.10	0.52	1.59	3.29
	10-35-0.67-2.79-ND	3000	2000	200	300	300	300	250	2.79	1.6	0.57	0.15	315	ND	10.0	35	0.11	0.40	1.71	2.96
	10-35-0.50-1.79-ND	3000	1500	200	300	300	300	250	1.79	1.6	0.57	0.15	315	ND	10.0	35	0.13	0.50	1.56	2.98
	10-35-0.50-2.79-ND	3000	1500	200	300	300	300	250	2.79	1.6	0.57	0.15	315	ND	10.0	35	0.14	0.31	1.65	5.02
	12-25-0.67-1.79-ND	3000	2000	200	300	300	300	250	1.79	1.6	0.57	0.15	225	ND	12.5	25	0.11	0.59	2.23	4.89
	12-25-0.67-2.79-ND	3000	2000	200	300	300	300	250	2.79	1.6	0.57	0.15	225	ND	12.5	25	0.10	0.43	2.31	3.22
	12-25-0.50-1.79-ND	3000	1500	200	300	300	300	250	1.79	1.6	0.57	0.15	225	ND	12.5	25	0.14	0.65	2.01	2.20
	12-25-0.50-2.79-ND	3000	1500	200	300	300	300	250	2.79	1.6	0.57	0.15	225	ND	12.5	25	0.14	0.63	1.97	2.48
	12-35-0.67-1.79-ND	3000	2000	200	300	300	300	250	1.79	1.6	0.57	0.15	315	ND	12.5	35	0.11	0.57	1.60	3.96
	12-35-0.67-2.79-ND	3000	2000	200	300	300	300	250	2.79	1.6	0.57	0.15	315	ND	12.5	35	0.11	0.42	1.71	2.89
	12-35-0.50-1.79-ND	3000	1500	200	300	300	300	250	1.79	1.6	0.57	0.15	315	ND	12.5	35	0.14	0.64	1.71	2.49
	12-35-0.50-2.79-ND	3000	1500	200	300	300	300	250	2.79	1.6	0.57	0.15	315	ND	12.5	35	0.12	0.44	1.65	3.15
Gap-07	17.5-25-1.33-1.31-D	3000	4000	200	350	350	300	250	1.31	1.6	0.22	0.15	306.25	D	17.5	25	0.07	0.25	0.32	3.94
	17.5-25-1.33-2.05-D	3000	4000	200	350	350	300	250	2.05	1.6	0.22	0.15	306.25	D	17.5	25	0.08	0.24	0.35	3.38
	17.5-25-1.00-1.31-D	3000	3000	200	350	350	300	250	1.31	1.6	0.22	0.15	306.25	D	17.5	25	0.09	0.23	0.36	3.40
	17.5-25-1.00-2.05-D	3000	3000	200	350	350	300	250	2.05	1.6	0.22	0.15	306.25	D	17.5	25	0.08	0.24	0.34	3.35
	17.5-35-1.33-1.31-D	3000	4000	200	350	350	300	250	1.31	1.6	0.22	0.15	367.5	D	17.5	35	0.07	0.34	0.29	2.96
	17.5-35-1.33-2.05-D	3000	4000	200	350	350	300	250	2.05	1.6	0.22	0.15	367.5	D	17.5	35	0.10	0.33	0.30	2.95
	17.5-35-1.00-1.31-D	3000	3000	200	350	350	300	250	1.31	1.6	0.22	0.15	367.5	D	17.5	35	0.11	0.36	1.52	3.37
	17.5-35-1.00-2.05-D	3000	3000	200	350	350	300	250	2.05	1.6	0.22	0.15	367.5	D	17.5	35	0.09	0.48	1.91	3.38
	20-25-1.33-1.31-D	3000	4000	200	350	350	300	250	1.31	1.6	0.22	0.15	306.25	D	20.0	25	0.09	0.25	0.32	3.79
	20-25-1.33-2.05-D	3000	4000	200	350	350	300	250	2.05	1.6	0.22	0.15	306.25	D	20.0	25	0.09	0.24	0.45	3.51
	20-25-1.00-1.31-D	3000	3000	200	350	350	300	250	1.31	1.6	0.22	0.15	306.25	D	20.0	25	0.08	0.23	0.50	3.49
	20-25-1.00-2.05-D	3000	3000	200	350	350	300	250	2.05	1.6	0.22	0.15	306.25	D	20.0	25	0.09	0.23	0.55	3.50
	20-35-1.33-1.31-D	3000	4000	200	350	350	300	250	1.31	1.6	0.22	0.15	367.5	D	20.0	35	0.06	0.29	1.18	2.21

	20-35-1.33-2.05-D	3000	4000	200	350	350	300	250	2.05	1.6	0.22	0.15	367.5	D	20.0	35	0.07	0.28	1.10	2.22
	20-35-1.00-1.31-D	3000	3000	200	350	350	300	250	1.31	1.6	0.22	0.15	367.5	D	20.0	35	0.07	0.27	1.20	2.23
	20-35-1.00-2.05-D	3000	3000	200	350	350	300	250	2.05	1.6	0.22	0.15	367.5	D	20.0	35	0.08	0.36	1.63	2.90
Gap-08	17.5-25-0.67-1.31-D	3000	2000	200	350	350	300	250	1.31	1.6	0.57	0.15	306.25	D	17.5	25	0.06	0.24	0.30	3.70
	17.5-25-0.67-2.05-D	3000	2000	200	350	350	300	250	2.05	1.6	0.57	0.15	306.25	D	17.5	25	0.06	0.23	0.33	3.10
	17.5-25-0.50-1.31-D	3000	1500	200	350	350	300	250	1.31	1.6	0.57	0.15	306.25	D	17.5	25	0.08	0.22	0.34	3.30
	17.5-25-0.5-2.05-D	3000	1500	200	350	350	300	250	2.05	1.6	0.57	0.15	306.25	D	17.5	25	0.08	0.23	0.33	3.34
	17.5-35-0.67-1.31-D	3000	2000	200	350	350	300	250	1.31	1.6	0.57	0.15	367.5	D	17.5	35	0.07	0.33	0.28	2.95
	17.5-35-0.67-2.05-D	3000	2000	200	350	350	300	250	2.05	1.6	0.57	0.15	367.5	D	17.5	35	0.09	0.32	0.29	2.94
	17.5-35-0.50-1.31-D	3000	1500	200	350	350	300	250	1.31	1.6	0.57	0.15	367.5	D	17.5	35	0.10	0.34	0.27	3.36
	17.5-35-0.50-2.05-D	3000	1500	200	350	350	300	250	2.05	1.6	0.57	0.15	367.5	D	17.5	35	0.08	0.45	1.51	3.38
	20-25-0.67-1.31-D	3000	2000	200	350	350	300	250	1.31	1.6	0.57	0.15	306.25	D	20.0	25	0.08	0.24	1.40	3.60
	20-25-0.67-2.05-D	3000	2000	200	350	350	300	250	2.05	1.6	0.57	0.15	306.25	D	20.0	25	0.08	0.22	0.45	3.48
	20-25-0.50-1.31-D	3000	1500	200	350	350	300	250	1.31	1.6	0.57	0.15	306.25	D	20.0	25	0.09	0.21	0.45	3.48
	20-25-0.50-2.05-D	3000	1500	200	350	350	300	250	2.05	1.6	0.57	0.15	306.25	D	20.0	25	0.10	0.21	0.48	3.40
	20-35-0.67-1.31-D	3000	2000	200	350	350	300	250	1.31	1.6	0.57	0.15	367.5	D	20.0	35	0.07	0.27	1.05	2.10
	20-35-0.67-2.05-D	3000	2000	200	350	350	300	250	2.05	1.6	0.57	0.15	367.5	D	20.0	35	0.08	0.28	0.90	2.10
	20-35-0.50-1.31-D	3000	1500	200	350	350	300	250	1.31	1.6	0.57	0.15	367.5	D	20.0	35	0.09	0.26	0.95	2.00
	20-35-0.50-2.05-D	3000	1500	200	350	350	300	250	2.05	1.6	0.57	0.15	367.5	D	20.0	35	0.09	0.33	1.53	2.50